QUASI-STEADY MPD PROPULSION AT HIGH POWER

A. C. Malliaris, R. R. John, R. L. Garrison and D. R. Libby

February 1971

Final Technical Report
AVSD-0146-71-RR
Prepared Under Contract No. NAS1-9939 by

AVCO CORPORATION
GOVERNMENT PRODUCTS GROUP
SYSTEMS DIVISION
Wilmington, Massachusetts 01887

for

NATIONAL AERONAUTICS AND SPACE ADMINISTRATION
Langley Research Center
Langley Station
Hampton, Virginia 23365

NASA CR-111872

QUASI-STEADY MPD PROPULSION AT HIGH POWER

A. C. Malliaris, R. R. John, R. L. Garrison and D. R. Libby

February 1971

Final Technical Report
AVSD-0146-71-RR
Prepared Under Contract No. NAS1-9939 by

AVCO CORPORATION
GOVERNMENT PRODUCTS GROUP
SYSTEMS DIVISION
Wilmington, Massachusetts 01887

for

NATIONAL AERONAUTICS AND SPACE ADMINISTRATION
Langley Research Center
Langley Station
Hampton, Virginia 23365

FOREWORD

This technical report was prepared by the Avco Corporation, Systems Division, Wilmington, Massachusetts, on Contract No. NAS1-9939 for the NASA/Langley Research Center, Langley Station, Hampton, Virginia. The work reported was accomplished under the technical cognizance of Mr. J. Hoell, Mr. J. Burlock and Mr. R. Hess. The authors express appreciation to these individuals for their active interest in the present work and for their many helpful suggestions.

ABSTRACT

This report documents an investigation of quasi-steady MPD propulsion at power levels in the range 1 to 10 megawatts. An axisymmetric configuration is used for the MPD thruster, (3 inch anode, 3/4 inch cathode), and a complete laboratory assembly provides current pulses in the range 5 to 50 kiloamperes and propellant pulses in the range zero to 30 gm/sec argon, with typical durations about 1 millisecond. In addition to argon, all other noble gases have been investigated as propellants. Empirical observations, supported also by an analytical discussion, show that the square of the MPD current divided by the mass flow rate is a very important parameter. This parameter has a critical limit, above which the operation of the thruster becomes increasingly unacceptable. This limit has been found to depend inversely on the square root of the molecular weight of the propellant.

Evaluation of the MPD thruster is carried out by means of MPD electrode calorimetry, flow velocity measurements, and impulse bit measurements. Numerous conclusions are drawn from data analysis. These conclusions are then summarized and their implications are examined regarding the performance of a high-power, quasi-steady MPD propulsion system. The most serious question, in the support subsystems, is the problem of energy storage in a capacitor bank. Detailed work, regarding tests and evaluation of commercially available capacitors, is reported in the Appendix.

TABLE OF CONTENTS

I. INTRODUCTION 1

II. LABORATORY ASSEMBLY OF A HIGH-POWER, PULSED MPD SYSTEM 3

A. Thruster Configuration 5
B. Pulsed Flow Rate 6
C. Energy Storage and Power Processing 8
D. Special Arrangement for Impulse Measurements 13

III. CRITICAL FLOW 15

A. Empirical Observations 15
B. Analytical Discussion 25
C. Concluding Remarks 34

IV. MPD ELECTRODE CALORIMETRY 36

V. MPD FLOW VELOCITY MEASUREMENTS 43

A. Introductory Remarks 43
B. Results and Discussion 44

1. Velocity measurements and I_{sp} determination at $(J^2/\dot{m})_{crit}$ 45
2. Velocity measurements and I_{sp} determination at values of $(J^2/\dot{m})$ other than critical 49

VI. IMPULSE MEASUREMENTS 53

A. The Measurement of Impulse Bits 53
B. Illustrative Examples of Impulse Measurements 61

VII. SUPPORT SUBSYSTEMS 63

VIII. CONCLUSIONS 66

REFERENCES 72

APPENDIX: TESTS AND EVALUATION OF COMMERCIALLY AVAILABLE CAPACITORS 75

ILLUSTRATIONS

Figure	1	Block diagram of the laboratory MPD system	4
	2a	Schematic presentation of a typical high-power, quasi-steady MPD thruster	6
	2b	Head-on view of a thruster, after many thousand pulses. The drilled, boron nitride backplate and the cathode tip may be seen through the orifice of the anode plate	7
	2c	Side view of a thruster assembly. From left to right: Anode plate, cylindrical plenum, backplate, valve and small propellant tank	7
	3	Schematic of the simple circuitry used to activate the pulsed valve for short $\dot{m}$ pulses	9
	4	Flow rate pulse (about 3 millisec long, about 2.2 gm/sec amplitude) generated with about 0.4 joules (stored in 20 microfarad at 200 volts). Note reproducibility in the overlay of 5 consecutive shots	9
	5	High-power, quasi-steady, MPD pulse. About 1.5 millisec at 32 kiloamperes and 22 gm/sec Argon	12
	6	MPD current (lower trace) and voltage pulses at 0.5 millisec/cm	17
	7	MPD current (lower trace) and voltage pulses at 0.5 millisec/cm	18
	8	MPD current (lower trace) and voltage pulses at 0.5 millisec/cm	20
	9	MPD current (lower trace) and voltage pulses at 0.5 millisec/cm	21
	10	MPD current (lower trace) and voltage pulses 0.5 millisec/cm	22
	11	MPD current (lower trace) and voltage pulses at 0.5 millisec/cm	23

ILLUSTRATIONS (Concl'd)

Figure 12 Critical values of J^2 versus $\dot{m}$ for three different propellants 24

13 Experimentally observed critical values of $(J^2/\dot{m})$ versus molecular weight. Comparison with $M^{-1/2}$ curve, normalized at argon 26

14 Experimentally observed critical values of $(J^2/\dot{m})$ versus molecular weight. Comparison with curve given by Eq. (7) 29

15 Data of Figure 13 or 14 plotted on a log-log graph 35

16 Fractional power losses in the MPD electrodes versus $(J^2/\dot{m})$ for argon 40

17 Equivalent electrode falls and MPD voltage versus $(J^2/\dot{m})$ for argon 41

18 Specific impulse from Doppler measurements versus molecular weight at critical $(J^2/\dot{m})$ 46

19 Specific impulse from Doppler measurements versus critical values of $(J^2/\dot{m})$ for several propellants 48

20 Specific impulse from Doppler measurements versus the parameter $(J^2/\dot{m})$ for argon 50

21 Measured impulse bit versus measured $\int J^2\,dt$ for argon 62

22 Specific impulse versus $(J^2/\dot{m})$. Comparison of velocity measurements (triangles) with preliminary impulse measurements (circles) for argon 69

TABLES

Table I Experimentally observed power at critical ($J^2/\dot{m}$) in the MPD flow versus the analytical prediction of Eq. (8) 30

II Numerical examples of MPD electrode calorimetry in argon. Average losses are established in the steady state from long runs of repetitive pulsing ... 39

III Most prominent spectral lines used in the Doppler experiments 44

IV Specific impulse at critical ($J^2/\dot{m}$) for argon 47

I. INTRODUCTION

The general objective of the work reported here is to establish the technical background necessary for the evaluation of a repetitively pulsed, high-power, quasi-steady MPD propulsion system. Particularly, the following topics are investigated:

(a) Design, assembly and tests of laboratory model of the aforementioned MPD system.

(b) Evaluation of the thruster operation at:

average powers 1 to 10 kilowatts

pulse powers 1 to 10 megawatts

pulse currents 3 to 50 kiloamperes

pulse durations of the order of 1 millisecond

rep rates of the order of 1 pps and with various propellants at rates between zero and 100 gm/sec

(c) Identification of critical aspects in the operation of the MPD thruster. Specifically, identification of current and flow rate limitations and the dependence of these limitations on the type of the propellant and on the geometry of the thruster.

(d) Evaluation of MPD losses by calorimetric techniques.

(e) Determination of MPD flow velocity by Doppler-shift measurements and identification of such measurements with the specific impulse, and

(f) Direct measurements of impulse bits and their evaluation.

After reporting this work, we review the conclusions and consider their implications with respect to the performance of the quasi-steady MDP thruster. Finally, we examine briefly the support subsystems and present in detail (see the Appendix) our findings regarding tests and evaluation of commercially available capacitors.

II. LABORATORY ASSEMBLY OF A HIGH-POWER, PULSED MPD SYSTEM

This system has been developed for tests and evaluation of repetitively pulsed MPD thrusters, under quasi-steady, high-power conditions. Generally, such a system includes an MPD thruster, a pulsed valve, an energy storage bank, power processing equipment and several auxiliary control devices. An overall view of the system is illustrated in the block diagram of fig. 1, with the main components on the right side of the figure, and the control devices on the left.

The master trigger provides initiating pulses either singly at will, or repetitively at rep rates in the range 0 to 10 pps. One part of the initiating pulse is used to provide a gate which turns the charging power switch off, for a short time, relative to the interval between pulses. A second part of the initiating pulse is delayed by delay No. 1. The delayed trigger then activates the pulsed valve through trigger box No. 3, and provides the $\dot{m}$ pulse. Furthermore, a further delay is necessary before the pulse power is triggered. This is provided by delay No. 2, which feeds trigger boxes 1 and 2, and thereby activates simultaneously the auxiliary breakdown of the MPD gap and the switch of the main power.

Straightforward versions of laboratory power supplies are employed for charging the capacitor bank, through a simple electro-mechanical switch. The capacitor bank is structured as a pulse forming network (PFN) and is described in the next section. The energy stored in the PFN is

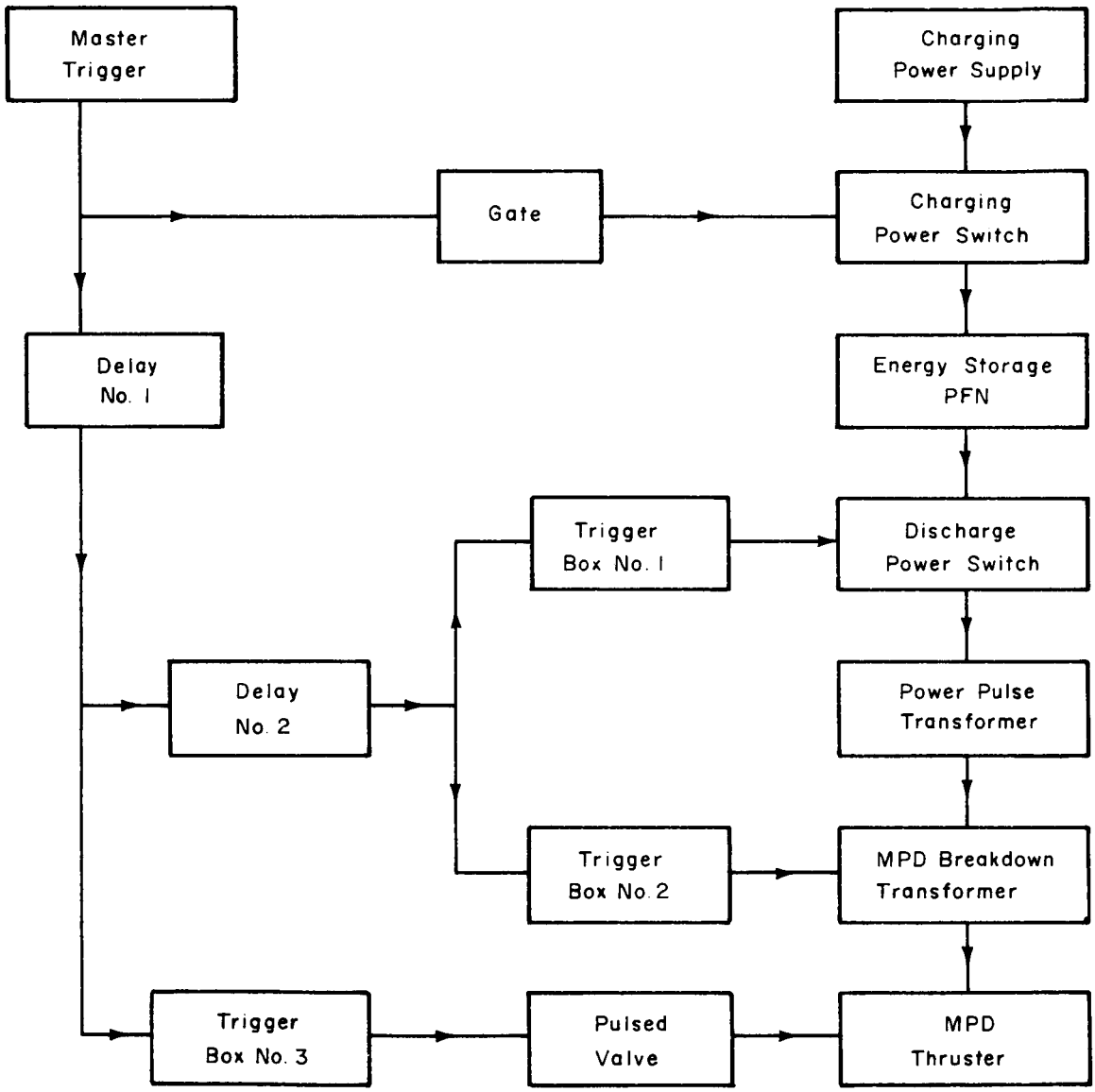

Figure 1 BLOCK DIAGRAM OF THE LABORATORY MPD SYSTEM

discharged, through an ignition switch, into the primary of a power pulse transformer. This transformer is naturally necessary for matching the pulsed MPD impedance to the PFN impedance. Finally, the role of the MPD Breakdown Transformer is to couple the MPD electrodes a high voltage (1000 to 2000 volts) low energy (few joules) pulse, which is employed for the auxiliary breakdown.

A. THRUSTER CONFIGURATION

The thrusters employed in this program have a configuration quite similar to those employed in recent studies of high-power, quasi-steady MPD accelerators. This is desirable to relate our work with the various studies and diagnostics, documented in refs. 1 to 6. A schematic presentation of a typical thruster is given in fig. 2a, and pictures of an actual thruster in use are presented in figs. 2b and 2c.

A typical plenum configuration is cylindrical, about 4 inches ID and 2 inches deep. It is lined with a quartz cylindrical insulator, 4 inches OD with a 2 millimeter wall thickness. The backplate of the plenum is also insulated by 1/8-inch thick boron nitride plate. This plate has about 24 evenly spaced holes (about 1/4-inch diameter) which allow the gas propellant to be fed to the acceleration region. A short drum (about 1/2-inch deep), not shown in fig. 2a, is situated behind the plenum backplate and is fed directly by the pulsed valve.

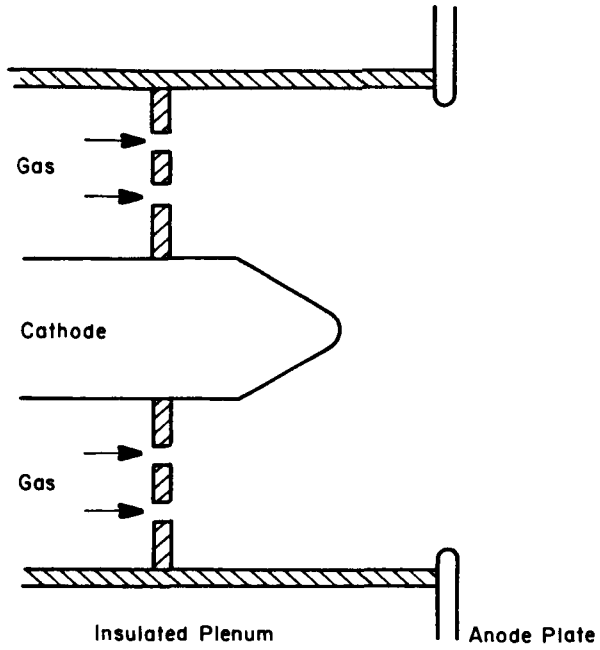

Figure 2a SCHEMATIC PRESENTATION OF A TYPICAL HIGH–POWER, QUASI–STEADY MPD THRUSTER

Typical cathode and anode configurations are evident in the sketch of fig. 2a. The cathode rod, 3/4-inch diameter, has a thoriated tungsten tip and is situated approximately midway in the plenum. The anode is a 1/4-inch copper plate with a 3-inch orifice and a 7-inch OD.

B. PULSED FLOW RATE

The importance of well defined pulses of propellant flow rate has been discussed in ref. 1. In the same reference the development of a pulsed valve assembly, from commercially available hardware, is described, and a detailed presentation is made of the diagnostics of the $\dot{m}$ pulses. Here we document briefly some additional developments.

One improvement has been the replacement of the power flip-flop, used to activate and deactivate the pulse valve. This has been replaced

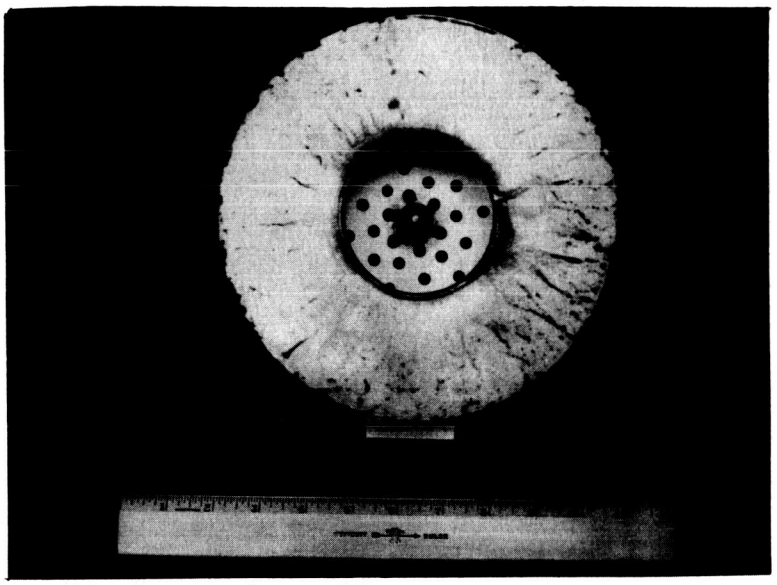

Figure 2b HEAD–ON VIEW OF A THRUSTER, AFTER MANY THOUSAND PULSES
The drilled, boron nitride backplate and the cathode tip may be seen through the orifice of the anode plate

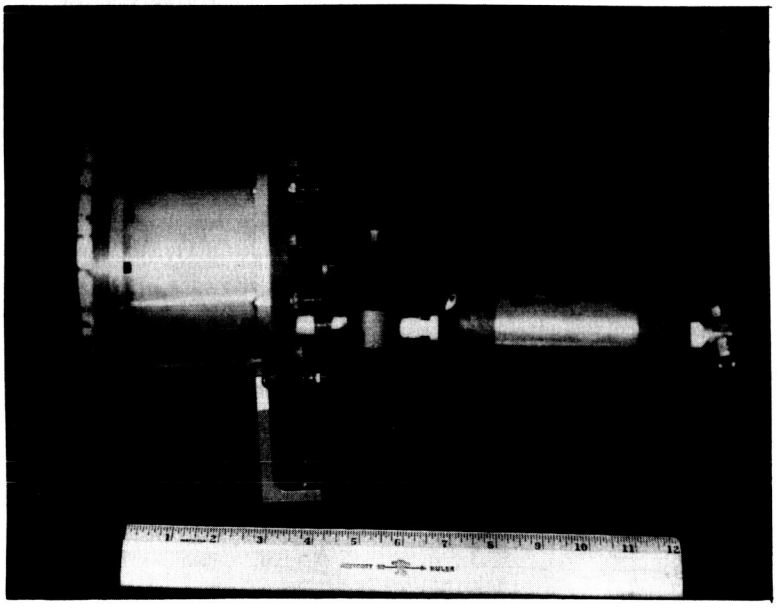

Figure 2c SIDE VIEW OF A THRUSTER ASSEMBLY
From left to right: Anode plate, cylindrical plenum, backplate, valve and small propellant tank

by the relatively simple circuitry shown in fig. 3. In essence here a capacitor, ranging from 10 to 100 microfarads, is charged at voltages 200 to 300 volts and then discharged through the valve coil. This may be done either singly at will, or repetitively at any desired rep rate. The valve is activated as soon as the capacitor discharge is initiated, and an automatic valve deactivation is provided when the capacitor has been discharged.

The advantages of this arrangement are numerous. The most important is the relatively short and well defined pulses of propellant flow, as illustrated in fig. 4. Additional advantages are simplicity, compactness, light weight and especially: a relatively small amount of energy for activation. Arrangements of this type have been used to provide fairly rectangular $\dot{m}$ pulses of a few millisecond duration and of amplitude in the range zero to 30 gm/sec for any gas. Extension to 100 gm/sec is straightforward.

C. ENERGY STORAGE AND POWER PROCESSING

In the main laboratory model of the pulsed MPD system, the pulse energy is stored in 20 x 200 microfarad capacitors rated up to 4000 volts. This total capacitance of 4000 microfarads is distributed in four sections of a pulse forming network (PFN) and may store a pulse energy up to 32 kilojoules.

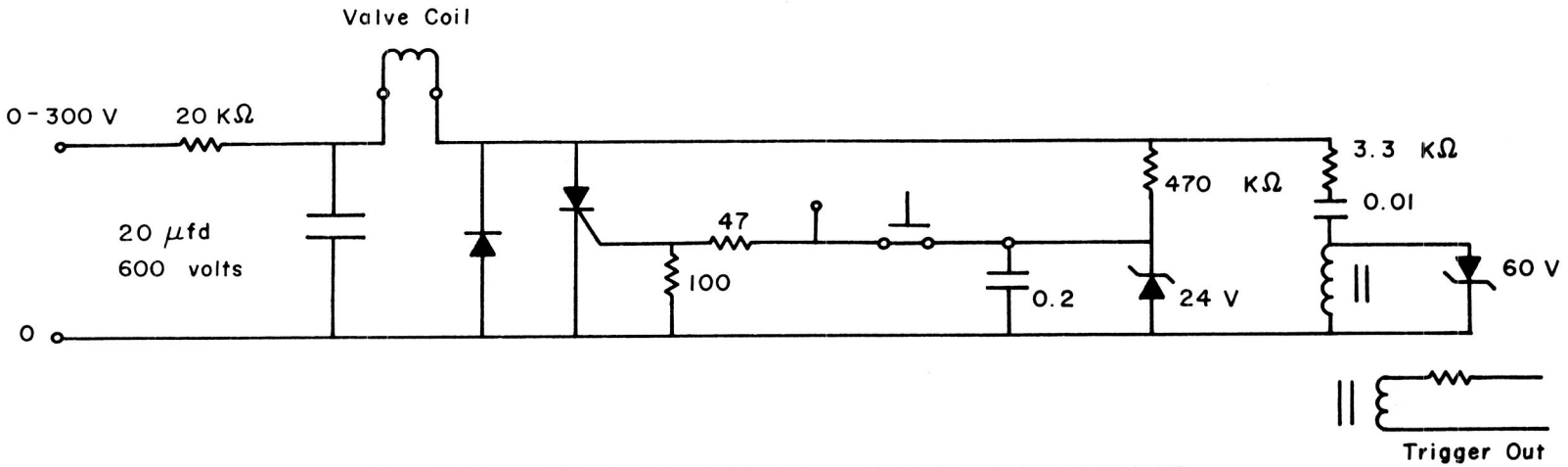

Figure 3 SCHEMATIC OF THE SIMPLE CIRCUITRY USED TO ACTIVATE THE PULSED VALVE FOR SHORT $\dot{m}$ PULSES

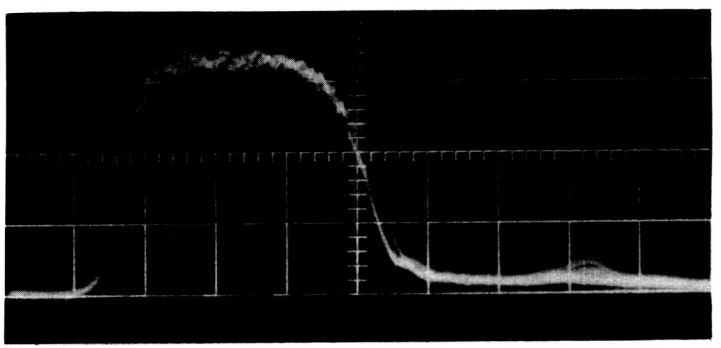

Figure 4 FLOW RATE PULSE (ABOUT 3 millisec LONG, ABOUT 2.2 gm/sec AMPLITUDE) GENERATED WITH ABOUT 0.4 joules (STORED IN 20 microfarad AT 200 volts)
Note reproducibility in the overlay of 5 consecutive shots

The PFN is a straightforward four section, voltage-fed network with about 1000 microfarads capacitance per section. Four identical, high Q, inductors are used and an inductance per section is available at the nominal values of 3, 7, 15, 30 and 60 microhenries per section. Under these conditions, the corresponding characteristic impedance of the PFN has the nominal values of 55, 84, 122, 173 and 245 milliohms. The corresponding power pulses have then the nominal durations of 0.44, 0.67, 1.0, 1.4 and 2.0 milliseconds.

It is quite evident that under such conditions a power pulse transformer is necessary for the matching of the aforementioned PFN impedances (which are quite high) to the MPD impedance (in the range 5 to 15 milliohms). Such a transformer has been designed by this laboratory, purchased and incorporated into the pulsed MPD system.

Briefly, the transformer has a 12 mil silectron core, with a cross-section 6 x 6 inches and a window 7 x 13 inches. There are two identical windings on each leg of the core. Each winding has four independent coils:

Secondary, 20 turns, 0.010 x 12-inch copper sheet

Primary, 10 turns, 0.030 x 12-inch copper sheet

Secondary, 20 turns, 0.010 x 12-inch copper sheet

Secondary, 40 turns, 0.010 x 12-inch copper sheet

Evidently, a very large variety of turn ratios (from 2:1 to 18:1) is available, and consequently, impedance transformation ratios of 4, 9, 16, 25, 36, 49, etc. are easily obtainable.

An example of pulses (current and voltage) is illustrated in fig. 5. The specifics here are as follows:

Total capacitance	4000 microfarads
Total Inductance	120 microhenries
PFN Impedance	173 milliohms
PFN Voltage	2500 volts
Stored Energy	12.5 kilojoules
Stored Charge	10 coulombs
Step-up Current Ratio	5
Impedance Transformer Ratio	25
Secondary Impedance	7 milliohms

It is seen that the power pulse is about 6.5 megawatts, and the following consistency checks may be applied. The power waveform (product of the two waveforms in fig. 1) integrated over the pulse duration gives about 10 kilojoules, which agrees fairly well with the total energy stored in the PFN. The small difference is accounted for by losses in the switch, transformer windings, leads, etc. Furthermore, the current waveform may also be integrated over the duration of the pulse. If the (secondary/primary) current ratio of 5 is taken into account, it is found

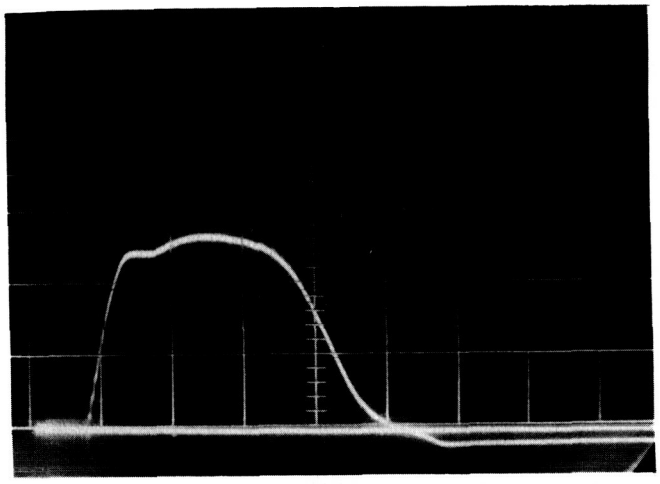

MPD Current Pulse
12.5 KA/cm, 0.5 millisec/cm

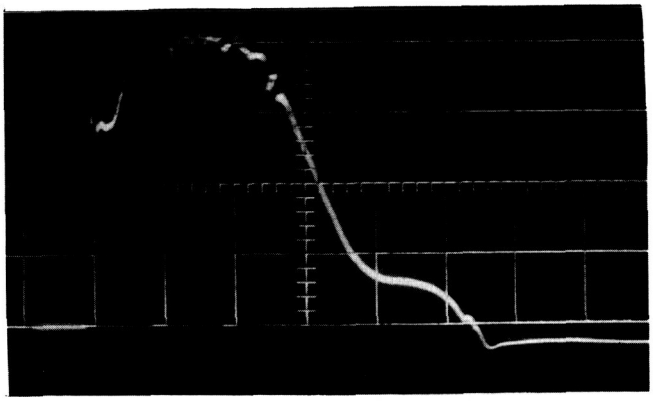

MPD Voltage Pulse
50 V/cm, 0.5 millisec/cm

Figure 5 HIGH–POWER, QUASI–STEADY, MPD PULSE
About 1.5 millisec at 32 kiloamperes and
22 gm/sec Argon

that the total charge is about 10 coulombs, which agrees very well with the amount of stored charge.

The present arrangement (i.e., the 173 milliohm PFN and the 25 to 1 transformation ratio) has a transformed impedance of 7 milliohms and has been used extensively in most of the work described in this report. In this work, the MPD impedance varies between 5 and 10 milliohms and the relative mismatch is generally acceptable.

D. SPECIAL ARRANGEMENT FOR IMPULSE MEASUREMENTS

For well understood reasons, whenever impulse measurements are necessary, all the energy storage and power conditioning equipment must be mounted with the thruster on the impulse measuring device, in the environmental tank. However, this equipment, as described in the previous section, has a weight and size too large to be accommodated within any reasonable facility. For this reason, special arrangements have been made for energy storage of power processing of the MPD system, which is used for impulse measurements. First, the need of the very heavy and bulky pulse transformer has been eliminated by replacing the previously described PFN with another, having a much lower characteristic impedance.

In this arrangement, the pulse energy is stored in a total capacitance of 0.18 farads (96 electrolytic capacitors, each 1900 microfarads, rated at 400 volts). An energy up to 15 kilojoules may be stored for each pulse. These capacitors, together with a total inductance in the

range 5 to 10 microhenries, form a PFN with a characteristic impedance in the vicinity of 7 milliohms and a characteristic pulse duration of about 2 milliseconds. This situation is quite acceptable for the high-power, quasi-steady MPD. Moreover, as may be seen, the PFN impedance is quite close to the typical MPD impedances. Consequently, no pulse transformer is required, and the whole assembly is sufficiently light (about 200 lbs) for mounting on an impulse measuring device.

III. CRITICAL FLOW

Consider an MPD accelerator operating with a propellant flow rate $\dot{m}$ at a current J. The work reported in this section is related to several very important questions, namely: Is there a critical value of $(J^2/\dot{m})$? Specifically, what is the maximum value of $(J^2/\dot{m})$ above which the MPD discharge is starved? Moreover, if there is a value of $(J^2/\dot{m})$ which demarks starvation, how does it depend on the type of the propellant? Furthermore, does it depend on the MPD geometry?

A. EMPIRICAL OBSERVATIONS

Experimental work at several laboratories and collective interpretation of experimental results has established that, for argon, the value of $(J^2/\dot{m}) \simeq 40\ (KA)^2/gm,\ sec^{-1}$ appears to be critical. This value, for argon, is considered as a demarkation of the onset of starvation. In other words, when $(J^2/\dot{m})_{argon} > 40\,(KA)^2/gm,\ sec^{-1}$, the MPD is underfed. The consequences may be ingestion of environmental and/or eroded material.

The aforementioned critical value has been established mainly on grounds of very unreasonable and very unacceptable consequences, arising when the participation of unmetered propellant is not allowed. (See for example refs. 5, 7 and 8, where some unrealistic and unacceptable results are obtained (in the energy and/or momentum balance of the MPD flow) when the $(J^2/\dot{m})$ parameter exceeds a value 30 to 50 $(KA)^2/gm,\ sec^{-1}$ for argon propellant.)

For reasons of clarity, we shall designate the region of high values of $(J^2/\dot{m})$ as the starvation region of the MPD operation. This implies that $\dot{m}$ is too low for a given current or alternatively that the current J is too high for a given $\dot{m}$. Similarly, we shall designate as overfed an MPD thruster for which $(J^2/\dot{m})$ has a value substantially lower than the critical value.

It should be noted that the experimental evidence mentioned above does not show a sharp and clear-cut transition from the overfed to the underfed condition. Similarly, a gradual instead of a sharp transition is observed in the erosion of thruster material as the value of $(J^2/\dot{m})$ is continuously increased.

In our experimental MPD thruster, we have replaced the plenum insulators (made previously of plastic) with quartz and boron nitride, which are not easily ablated. We have thus appreciably reduced the amount of thruster material which could be ingested as propellant. With this background in mind, we proceeded to observe whether any signs of discomfort and instability are manifested, as soon as operation is attempted at values of $(J^2/\dot{m})$ above the critical.

Representative results for argon are illustrated in figs. 6 and 7. Each frame in these figures presents two traces. The upper trace is the voltage at 50 volts/cm, while the current is displayed in the lower trace at about 5 KA/cm. Both traces, at 0.5 millisec/cm, have a common time origin.

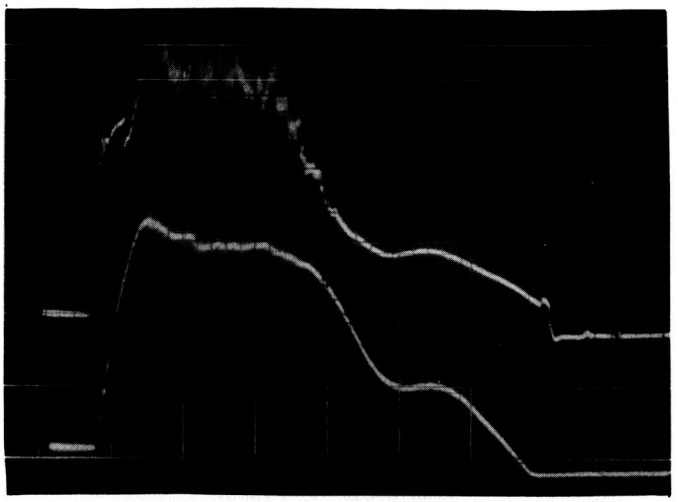

$\dot{m}$ = 3.6 gm/sec Argon

J = 15 KA

$(J^2/\dot{m})$ = 63 $(KA)^2$ /gm, sec^{-1}

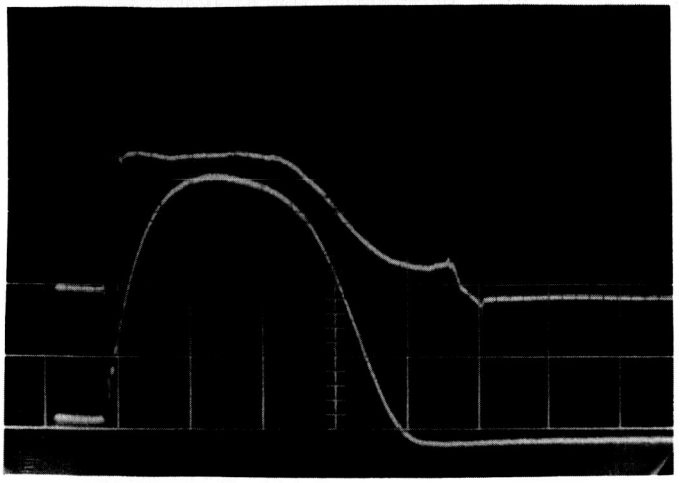

$\dot{m}$ = 7.5 gm/sec Argon

J = 17 KA

$(J^2/\dot{m})$ = 38 $(KA)^2$ /gm, sec^{-1}

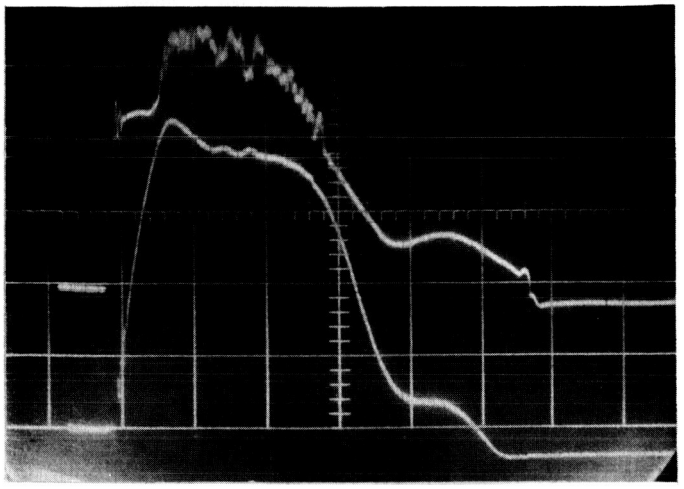

$\dot{m}$ = 7.5 gm/sec Argon

J = 19 KA

$(J^2/\dot{m})$ = 48 $(KA)^2$ /gm, sec^{-1}

Figure 6 MPD CURRENT (LOWER TRACE) AND VOLTAGE PULSES AT 0.5 millisec/cm

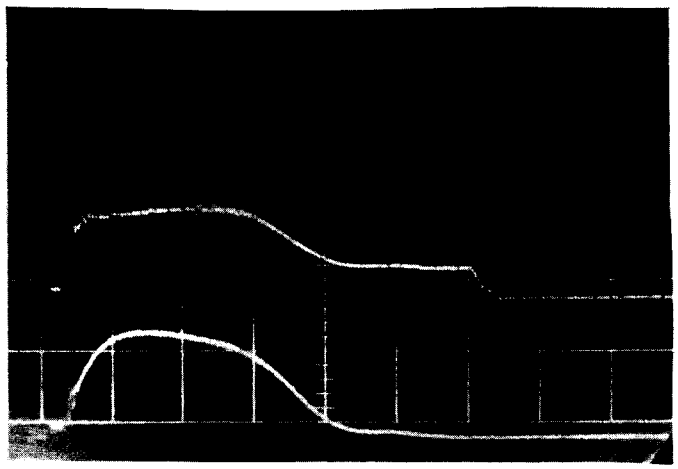

$\dot{m}$ = 1.4 gm/sec Argon

J = 6 KA

$(J^2/\dot{m})$ = 26 $(KA)^2$ gm, sec^{-1}

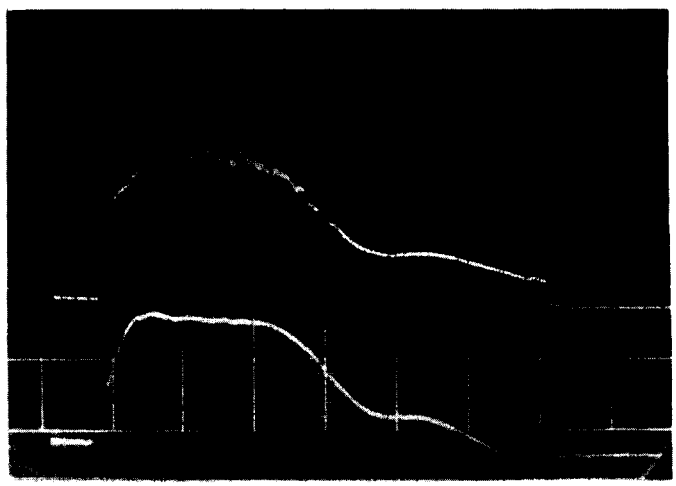

$\dot{m}$ = 1.4 gm/sec Argon

J = 8 KA

$(J^2/\dot{m})$ = 46 $(KA)^2/gm, sec^{-1}$

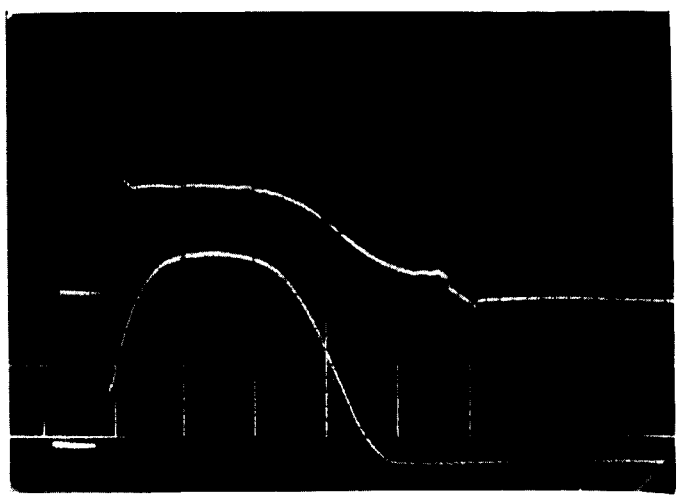

$\dot{m}$ = 7.5 gm/sec Argon

J = 13 KA

$(J^2/\dot{m})$ = 23 $(KA)^2/gm, sec^{-1}$

Figure 7 MPD CURRENT (LOWER TRACE) AND VOLTAGE PULSES AT 0.5 millisec/cm

It is obvious in the examples of figs. 6 and 7 that whenever $(J^2/\dot{m})$ exceeds the value of 40 $(KA)^2/gm, sec^{-1}$ (believed to be the critical value for argon) the MPD voltage jumps very substantially and becomes clearly unstable. This is so for virtually any combination of J^2 and $\dot{m}$ that has a ratio larger than the aforementioned critical value. The transition, interpreted tentatively as the onset of starvation, appears to be quite sharp, as may be seen by comparing the middle with the lower frame in fig. 6.

Motivated by these observations, we decided to extend these experiments over a wide range of available propellants. Representative results are illustrated in figs. 8 to 11 for xenon, neon, krypton and helium. In all cases, critical values of $(J^2/\dot{m})$ were found, which depend roughly on the molecular weight to the minus one-half power. Results for diatomic and polyatomic molecules, e.g., N_2, NH_3, etc., are not as clear-cut as for the noble gases.

The general range of conditions (i.e., J^2 and $\dot{m}$ values) is shown in fig. 12, which illustrates the critical values of J^2 versus $\dot{m}$ for three different propellants. It is easily checked that $(J^2/\dot{m})$ has a constant value, which depends on the propellant only. In fig. 12, the upper-left region is identified as the starvation region, while overfeed should be associated with the lower right. The demarkation between the two regions is provided by the straight line, for each propellant, which defines the so-called critical value of $(J^2/\dot{m})$.

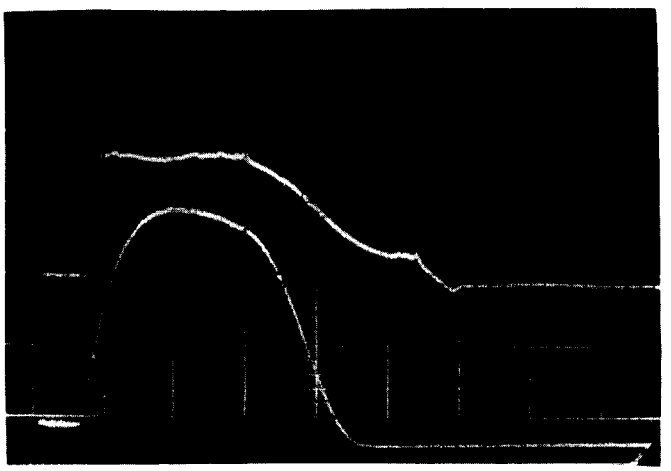

$\dot{m}$ = 13.0 gm/sec Xenon

J = 14.5 KA

$(J^2/\dot{m})$ = 16 $(KA)^2/gm, sec^{-1}$

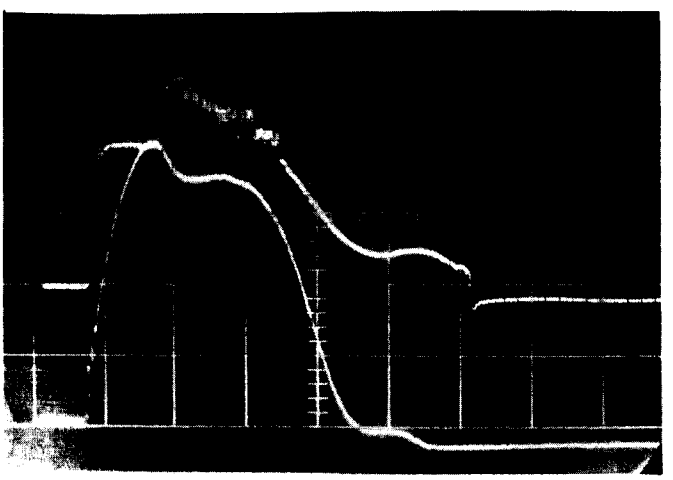

$\dot{m}$ = 13.0 gm/sec Xenon

J = 17 KA

$(J^2/\dot{m})$ = 22 $(KA)^2/gm, sec^{-1}$

Figure 8 MPD CURRENT (LOWER TRACE) AND VOLTAGE PULSES AT
0.5 millisec/cm

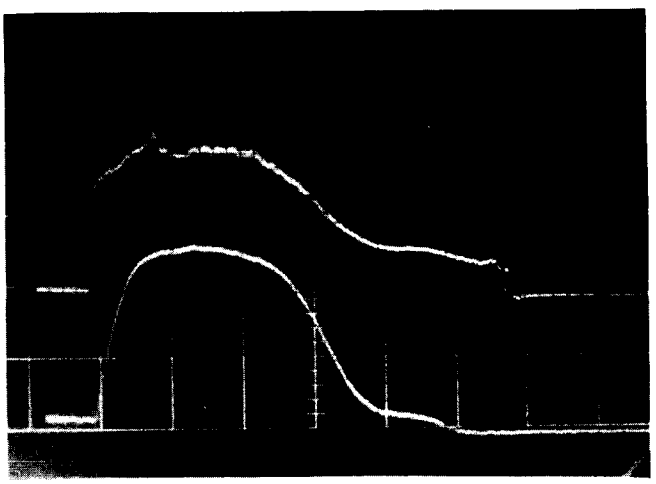

$\dot{m}$ = 2.5 gm/sec Neon

J = 12 KA

$(J^2/\dot{m})$ = 58 $(KA)^2/gm, sec^{-1}$

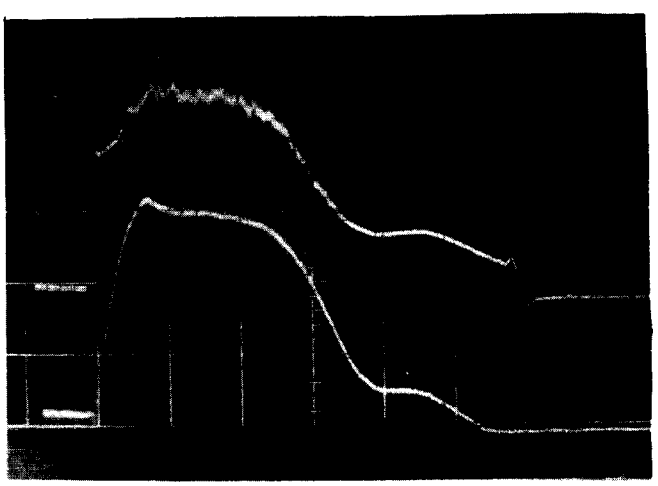

$\dot{m}$ = 2.5 gm/sec Neon

J = 14.5 KA

$(J^2/\dot{m})$ = 84 $(KA)^2/gm, sec^{-1}$

Figure 9 MPD CURRENT (LOWER TRACE) AND VOLTAGE PULSES AT
0.5 millisec/cm

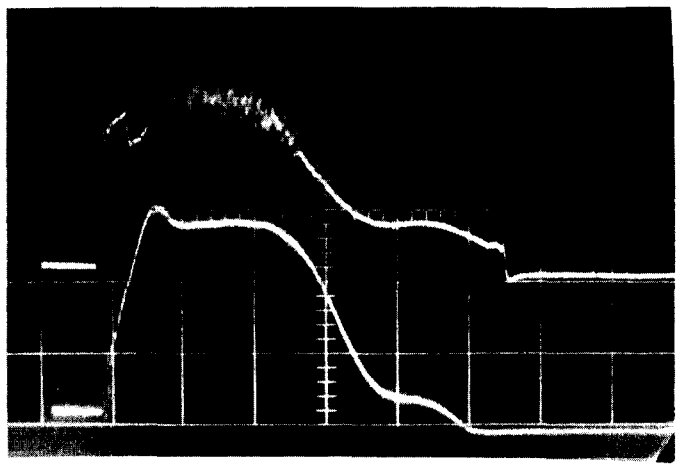

$\dot{m}$ = 5.2 gm/sec Krypton

J = 14 KA

$(J^2/\dot{m})$ = 38 $(KA)^2/gm, sec^{-1}$

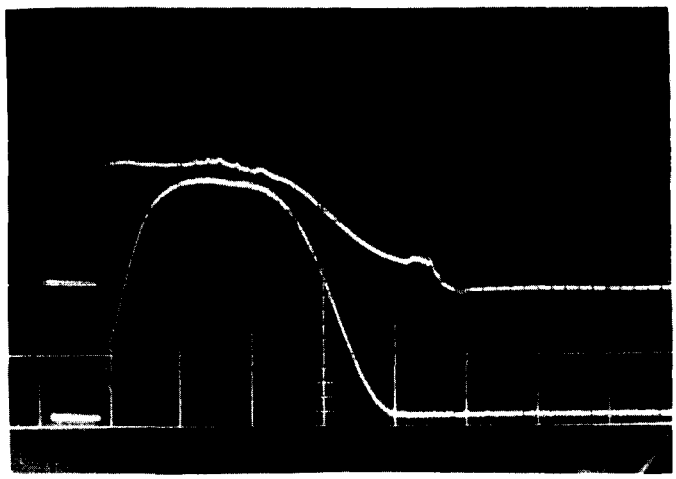

$\dot{m}$ = 11.0 gm/sec Krypton

J = 16.5 KA

$(J^2/\dot{m})$ = 25 $(KA)^2/gm, sec^{-1}$

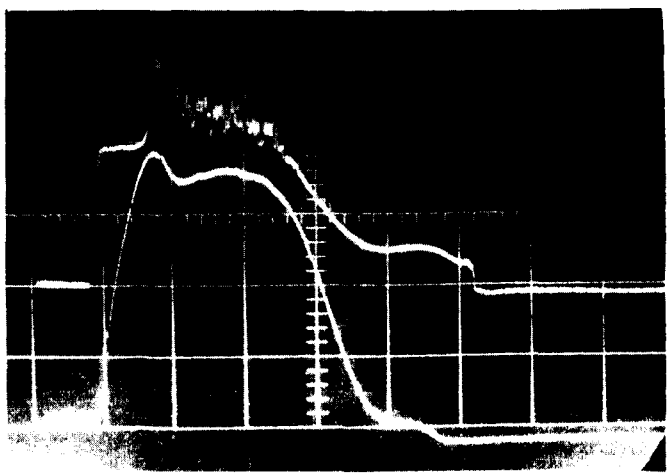

$\dot{m}$ = 11.0 gm/sec Krypton

J = 17.5 KA

$(J^2/\dot{m})$ = 28 $(KA)^2/gm, sec^{-1}$

Figure 10 MPD CURRENT (LOWER TRACE) AND VOLTAGE PULSES AT 0.5 millisec/cm

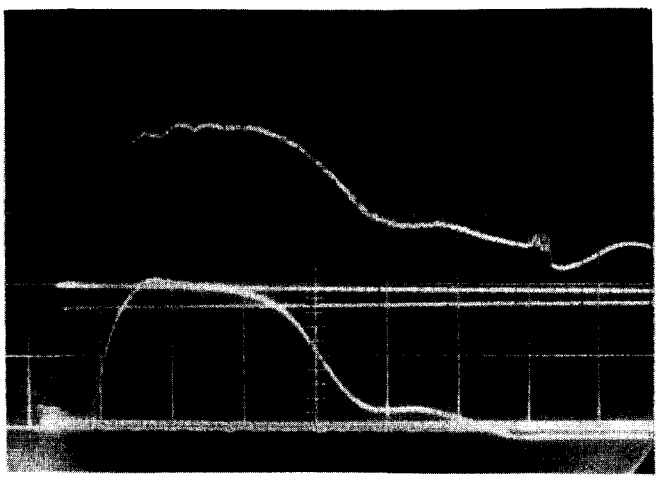

$\dot{m}$ = 1.2 gm/sec Helium

J = 10 KA

$(J^2/\dot{m})$ = 84 $(KA)^2$ /gm, sec^{-1}

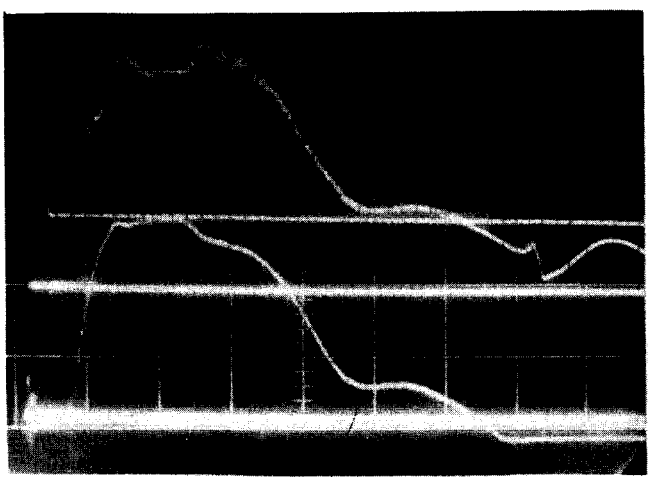

$\dot{m}$ = 1.2 gm/sec Helium

J = 14.5 KA

$(J^2/\dot{m})$ = 175 $(KA)^2$/gm, sec^{-1}

Figure 11 MPD CURRENT (LOWER TRACE) AND VOLTAGE PULSES AT 0.5 millisec/cm

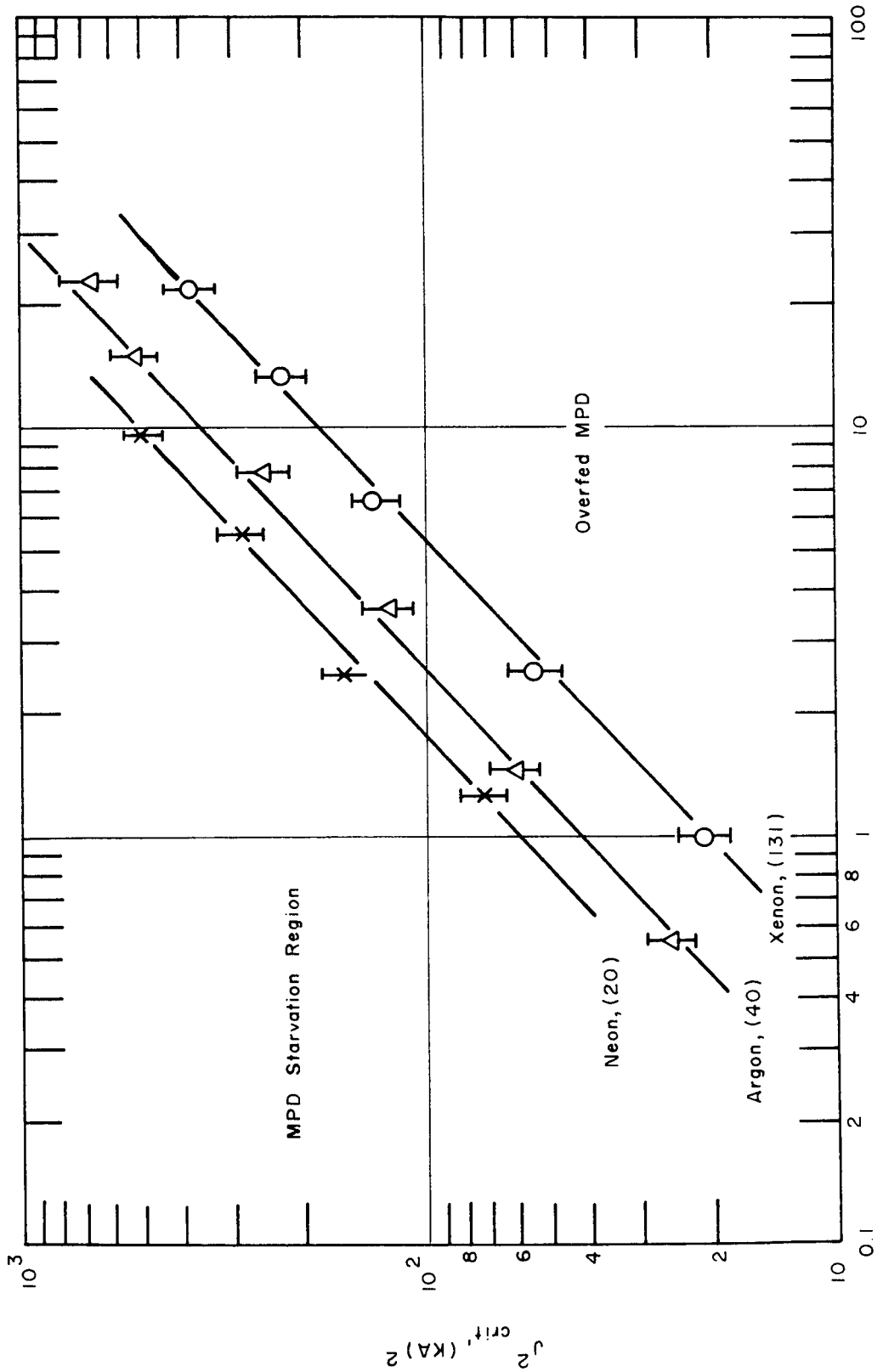

Figure 12 CRITICAL VALUES OF J^2 VERSUS $\dot{m}$ FOR THREE DIFFERENT PROPELLANTS

B. ANALYTICAL DISCUSSION

The aforementioned experimental results are summarized in fig. 13, where we plot the observed critical values of $(J^2/\dot{m})$ versus the molecular weight, M. The curve fit in this figure represents a $(M^{-1/2})$ dependence, fitted arbitrarily for argon. Good agreement is obvious.

Because of this good agreement, and because of the substantial additional and independent evidence for argon (refs. 5, 7 and 8), we would like to outline here an analytical discussion which, although not thoroughly understood, provides a very interesting background.

Consider Eq. (1):

$$P_{flow} = (\dot{m}/M) \cdot N_o \cdot e\ V_i + (F^2/2\dot{m}) \qquad (1)$$

where: P_{flow} represents the power invested in the flow; $\dot{m}$, M and V_i are respectively the mass flow rate, the molecular weight and ionization potential of the propellant; and F is the self-magnetic force (not necessarily the thrust). N_o and e are constants having respectively the values: 6×10^{23} particles/mole and 1.6×10^{-19} MKS/electron charge.

The second term in Eq. (1) represents the kinetic power of the flow, while the first term is responsible for the power expended for ionization. (The thermal power is considered relatively unimportant.) In essence then, we have assumed, in Eq. (1), that the flow has two principal degrees of freedom which share the flow power P_{flow}. This

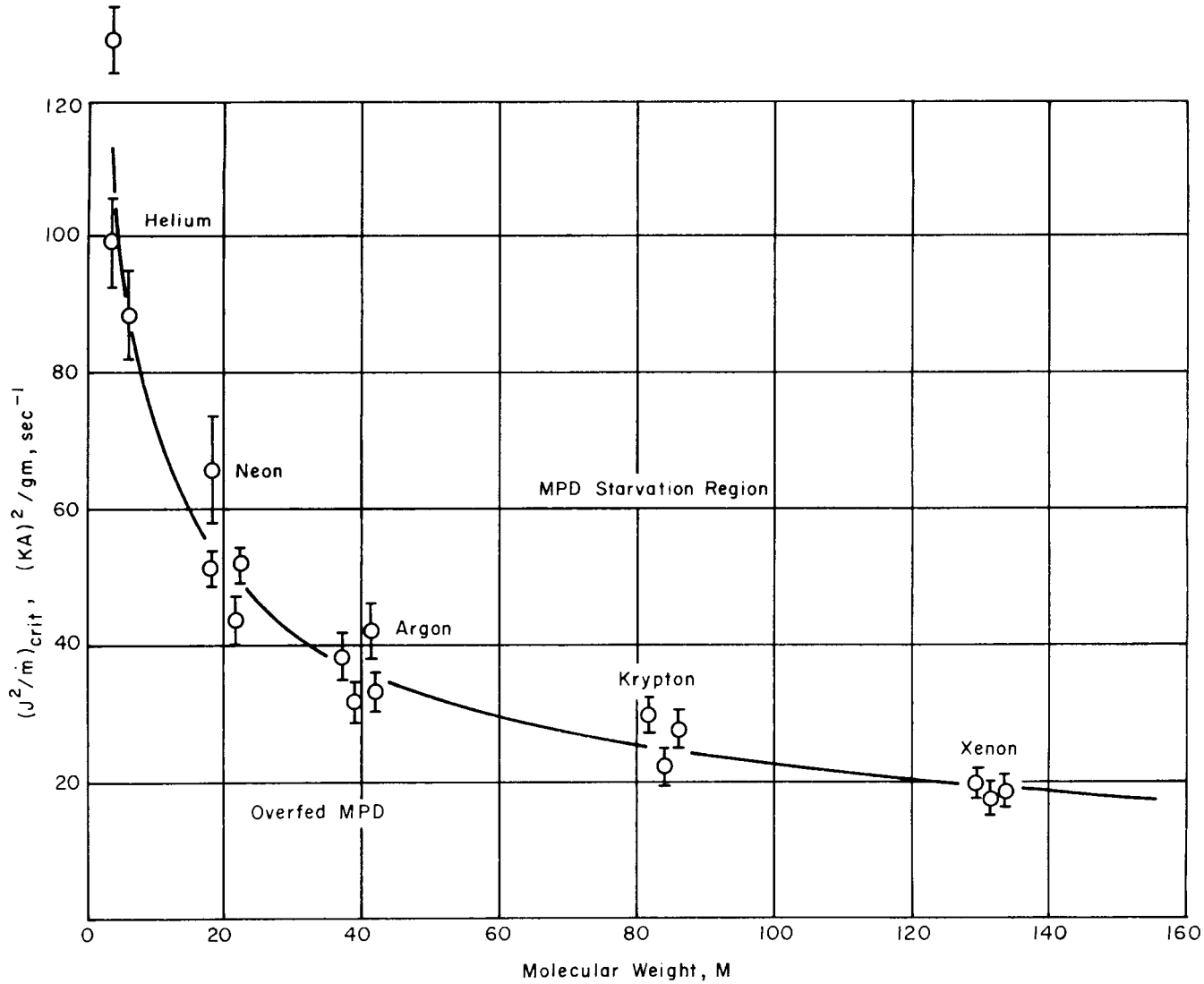

Figure 13 EXPERIMENTALLY OBSERVED CRITICAL VALUES OF $(J^2/\dot{m})$ VERSUS MOLECULAR WEIGHT
Comparison with $M^{-1/2}$ Curve, Normalized at Argon

power should be the electrical input power, reduced by the electrode losses and possibly by radiation losses.

Under otherwise fixed conditions we see that P_{flow}, in Eq. (1), depends on $\dot{m}$. Moreover, we may expect a relatively stable MPD condition when P_{flow} is minimized, (minimum discharge voltage), in other words when:

$$(\partial P_{flow} / \partial \dot{m}) = 0 \tag{2}$$

From Eqs. (1) and (2) we easily obtain:

$$(\dot{m}/M)\ N_o\ e\ V_i = F^2/2\dot{m} \tag{3}$$

$$(F/\dot{m}) = (2 e N_o)^{1/2}\ (V_i/M)^{1/2} \tag{4}$$

Furthermore, we recall the expression which gives the self-magnetic force, F, in terms of the MPD current J, and geometry:

$$F = b J^2 \tag{5}$$

$$b = 10^{-7}\ [(1/2) + \ell n\ (r_A/r_C)],\ \text{MKS} \tag{6}$$

where r_A and r_C are the MPD anode and cathode radii. An analytical expression for the parameter $(J^2/\dot{m})$ may be derived now by a combination of Eqs. (4) and (5):

$$(J^2/\dot{m})_{crit} = [(2 e N_o)^{1/2}/b] \cdot (V_i/M)^{1/2} \tag{7}$$

We may now plot this analytical expression of $(J^2/\dot{m})$ versus the propellant properties. For this, we need a numerical value for the MPD geometry constant, b. In our case (3-inch anode radius, 3/4-inch cathode), b equals approximately 2×10^{-7} MKS. Accordingly, we obtain the curve given in fig. 14. Here we compare Eq. (7) with the experimental observations summarized in the last section.

As may be seen in fig. 14, the agreement of the experimental data with the curve given by Eq. (7) is quite good. However, we consider this agreement at best fortuitious, in view of the crudeness of the analytical model. Further concern, regarding the crudeness of the analytical model, arises when we consider the power in the flow, given by Eq. (1). When condition (2) is satisfied, then the power in the flow has a value P_c, which is designated here as critical, simply because it corresponds to the critical value of $(J^2/\dot{m})$. It follows from Eqs. (1), (3), (5) and (7) that:

$$P_c = 2 N_o e (V_i/M) \dot{m} - (F^2/\dot{m}) - b^2 (J^2/\dot{m})_{crit} J^2 \qquad (8)$$

where $(J^2/\dot{m})_{crit}$ is the critical value given by (7).

We may now compare the analytical prediction of Eq. (8) with experimentally derived values of the power in the flow. This is done in table I. In this table, we consider representative cases and we calculate the electrical input power JV. From this, we obtain an estimate

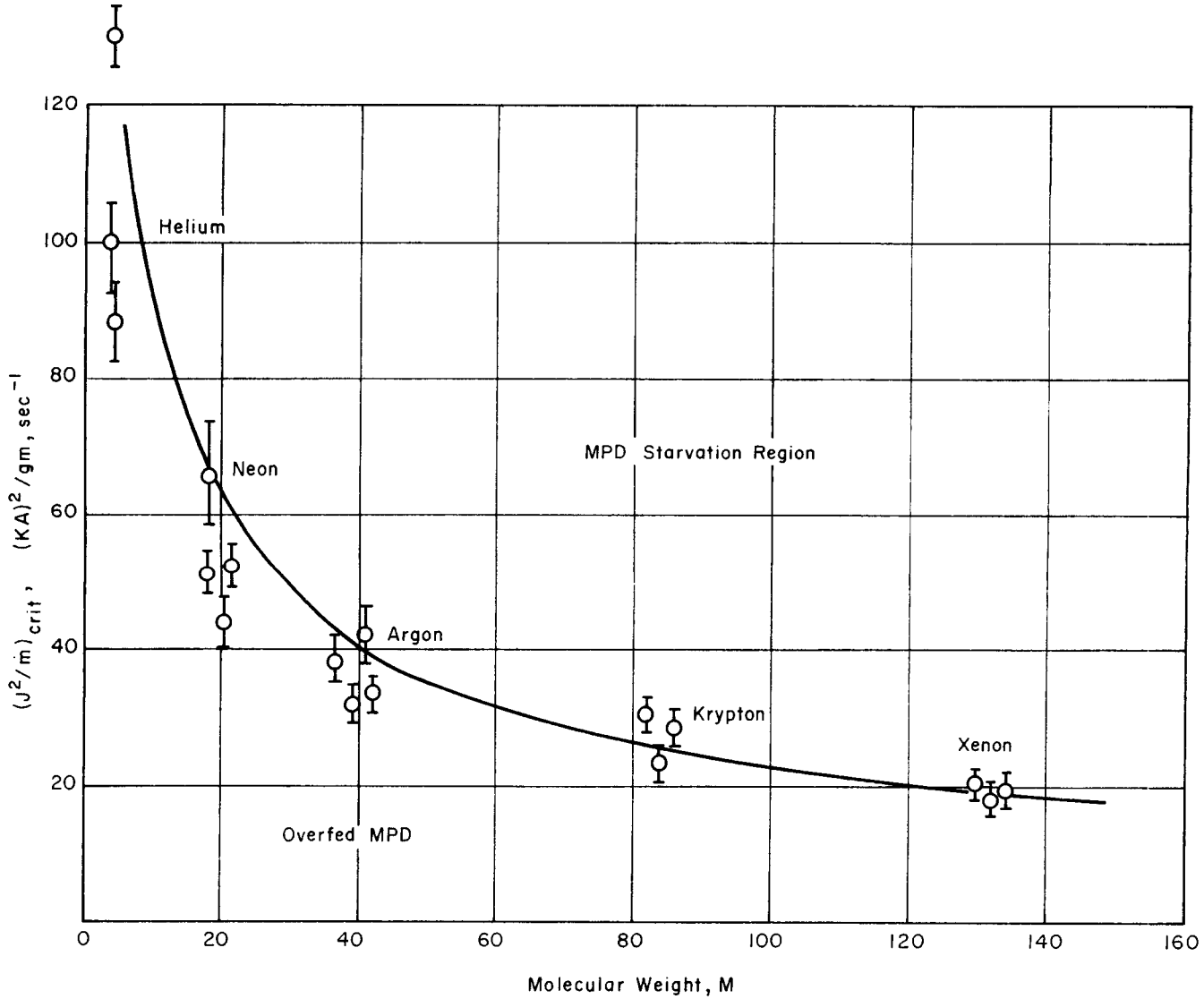

Figure 14 EXPERIMENTALLY OBSERVED CRITICAL VALUES OF $(J^2/\dot{m})$ VERSUS MOLECULAR WEIGHT
Comparison with Curve Given by Eq. (7)

TABLE I

EXPERIMENTALLY OBSERVED POWER AT CRITICAL ($J^2/\dot{m}$) IN THE MPD FLOW VERSUS THE ANALYTICAL PREDICTION OF EQ. (8).

Case	Gas	$(J^2/\dot{m})$, $(KA)^2/gm,sec^{-1}$	$\dot{m}$, gm/sec	J, KA	V, volts	JV, kilowatts	P′, kilowatts	P_c, kilowatts
	Argon	38	7.5	17.0	95	1600	720	440
	Xenon	16	13.0	14.5	80	1150	520	135
	Neon	58	2.5	12.0	95	1140	510	335
	Krypton	25	11.0	16.5	85	1400	630	270
	Helium	84	1.2	10.0	110	1100	490	340
	Helium	175	1.2	14.5	150	2150	970	1470

of the power in the flow, after subtracting about 55 percent to account for losses.* These experimentally estimated values are designated by P' and are tabulated in table I. The last column in this table gives the value of the analytical expression of Eq. (8).

It is obvious that the results of this comparison are only partially satisfactory. However, as will be seen in the following discussion, a relatively poor prediction of P_c does not necessarily imply a poor prediction of $(J^2/\dot{m})_{crit}$.

We make here a few remarks regarding this discrepancy. Our first remark is that each of the two terms appearing in Eq. (1), is a very crude approximation. The first term, for example, assumes that all the propellant $\dot{m}$ is ionized and that each ionization requires an energy corresponding to the ionization potential, V_i . A more realistic approximation should require a factor: $(f_1 g_1 + f_2 g_2 + f_3 g_3)$ to appear in front of the first term in Eq. (1). In other words the power input, (other than kinetic), into the gas should be given by:

$$(f_1 g_1 + f_2 g_2 + f_3 g_3) \cdot (\dot{m}/M) \cdot N_o \cdot e\ V_i)$$

where f_1 , f_2 and f_3 are fractions of $\dot{m}$, varying from zero to 100 percent. Each of these fractions corresponds to ionization, dissociation (if applicable), and heating. The factors g_1 , g_2 and g_3 , appearing in the above expression, correspond to the amount of energy required for

*This figure for losses is not arbitrary. As will be seen later, the calorimetric measurements reported here justify this general level of losses for the range of conditions in table I.

ionization, dissociation and heating (expressed in terms of the ionization potential). Moreover, the heating term may be expanded to include radiation losses, if necessary.

As an example, consider a case with 90 percent ionization (i.e., $f_1 = 0.9$) and assume that the generation of each ion pair requires twice the ionization potential energy (i.e., $g_1 = 2$). Ignoring dissociation, and assuming that all the propellant (ions, electrons and neutrals) is heated to a temperature about (1/10) of the ionization potential, we arrive at a value of $(f_1 g_1 + f_2 g_2 + f_3 g_3)$ approximately equal to 2.

Similar remarks may be made regarding the kinetic part of the power input. Thus in Eq. (1), we assumed that the force, F, acts uniformly on all the propellant flow rate $\dot{m}$. Consequently, the required kinetic power input was $(F^2/2\dot{m})$. However, in reality it is more likely that the propellant flow rate acquires momentum in a nonuniform fashion. As we well know, the power required for this case is higher than $F^2/2\dot{m}$. For example, the kinetic power must be increased by about 50 percent, above the amount required for uniform acceleration, if about 10 percent of the propellant is accelerated to 4 times the velocity of the other 90 percent of the propellant, provided that in both cases the same force, F, acts on the total $\dot{m}$. Furthermore, note that not only the kinetic power corresponding to the electro-magnetic force, F, may be higher than $(F^2/2\dot{m})$, but other forces as well may be active, requiring additional power.

In essence, we may summarize our remarks here by noting that the power in the MPD flow may be written generally:

$$P_{flow} = (A\dot{m}) + (B/\dot{m}) \tag{9}$$

where the first term accounts for all power input (other than kinetic), while the second term is the kinetic power. Equation (1), discussed earlier, is a specific example of Eq. (9), in fact the simpler-most example. The power given by Eq. (9) is minimized, with respect to $\dot{m}$, when $\dot{m}$ has the so-called critical value:

$$\dot{m}_c = (B/A)^{1/2} \tag{10}$$

and the corresponding critical power is:

$$P_c = 2\,(AB)^{1/2} \tag{11}$$

It is evident in relations (10) and (11) that the critical value of $\dot{m}$, and thus of $(J^2/\dot{m})$, is much less sensitive to the actual values of A and B coefficients, than is the critical power; for example, consider B increased by a factor of 3 and A by a factor of 2. The resulting increase of P_c is by a factor of about 2.5, while $\dot{m}_c$ increases by only 22 percent. Accordingly, a fairly good prediction of $\dot{m}_c$, and thus of $(J^2/\dot{m})_{crit}$, is compatible with a very poor prediction of the corresponding P_c.

C. CONCLUDING REMARKS

Regardless of the agreement or disagreement of the experimental results with analytical predictions, we should keep in mind here that the experimental evidence indicates clearly the existence of a critical value of $(J^2/\dot{m})$, above which the MPD discharge becomes increasingly unstable and erratic. This demarkation also coincides with increasing evidence of erosion and/or ingestion and is tentatively identified here as the onset of the MPD starvation region. Moreover, the critical value of $(J^2/\dot{m})$ decreases monotonically, approximately as the square root of the molecular weight increases.

Figure 15 presents again our experimental results, and extrapolates the existent trend to the molecular weight of mercury. The implication here is clear. In MPD operation with heavy propellants, the undesirable starvation region may be avoided only at comparatively low values of $(J^2/\dot{m})$. Thus for any given current, the heavier propellants may be acceptable only at higher flow rates, and therefore at lower propulsion performance when compared with lighter propellants.

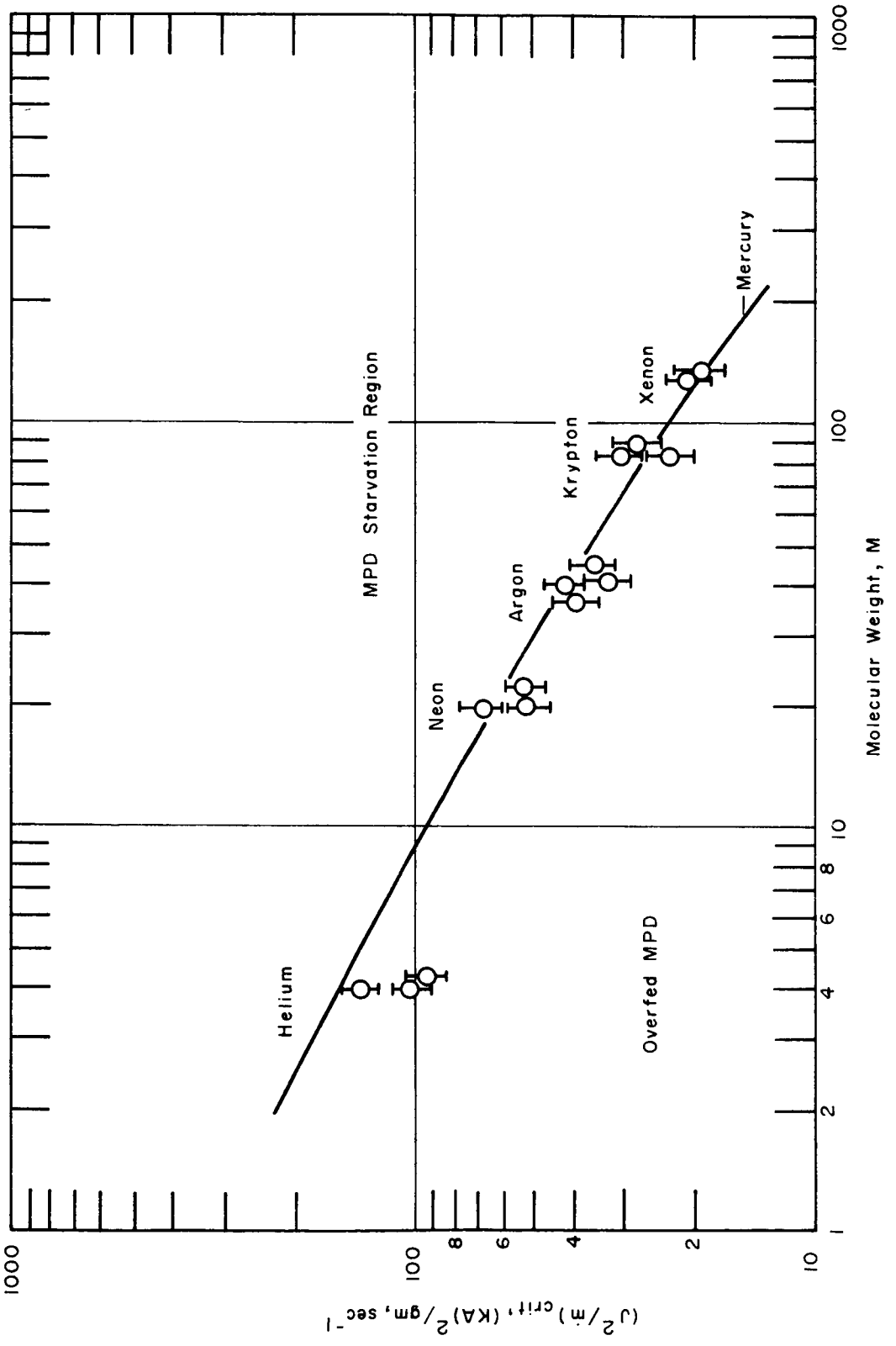

Figure 15 DATA OF FIGURE 13 OR 14 PLOTTED ON A LOG-LOG GRAPH

IV. MPD ELECTRODE CALORIMETRY

The determination of MPD electrode losses is a very important item in the evaluation of MPD thrusters. Naturally, the most reliable and straightforward way to determine these losses is by calorimetric techniques, especially of the steady-state type.

In the work reported here, the high-power, quasi-steady MPD thruster has been modified for electrode calorimetry, simply by making the appropriate water cooling provisions for the anode and cathode separately. In addition, provisions are also made for water flow rate measurements and for water temperature measurements.

In actual practice, we employ the MPD system described in Section II and pulse it repetitively, until the power lost to the cathode and to the anode reach steady state. Due to the substantial heat capacity of these electrodes, steady state is reached only after several minutes of continuous pulsing at rep rates of the order of 1 pps.

Each experimental run, at a preset rep rate r, includes the usual measurements of the mass flow rate $\dot{m}$, the MPD pulse current and voltage, J and V, and the pulse duration, t_d. Simultaneously, the electrode losses are monitored as a function of time, and when a steady state becomes evident, the average anode and cathode losses, $\langle Q_A \rangle$ and $\langle Q_C \rangle$ are measured.

From the pulse current and voltage, we derive the pulse power: $P = JV$. Moreover, the average power input is obtained from:

$$< P > = a P \tag{12}$$

where:

$$a = r \cdot t_d \tag{13}$$

is the duty cycle in the repetitive operation. Thus, the aforementioned measurements give us the:

$$\text{Fractional Anode Loss} = < Q_A > / < P > \tag{14}$$

and the:

$$\text{Fractional Cathode Loss} = < Q_C > / < P > \tag{15}$$

The fractional total loss is naturally the sum of Eqs. (14) and (15). Furthermore, we may derive the important parameters, namely the equivalent anode and cathode drops, as follows: If the average losses $< Q_A >$ and $< Q_C >$ are divided by the duty cycle, we obtain the corresponding losses during the pulse:

$$Q_A = < Q_A > / a \tag{16}$$

$$Q_C = < Q_C > / a \tag{17}$$

These losses may be thought of as the product of the pulse current time an equivalent voltage fall. Accordingly:

$$V_A = (Q_A / J) \tag{18}$$

and

$$V_C = (Q_C / J) \tag{19}$$

These relations are applied to our experimental data, which are summarized in table II. A total of six cases for argon are tabulated, each resulting from several repeated experimental runs. A reproducibility of ±15 percent has been observed. In the data of this table, we have selected MPD currents from about 7 to 16 kiloamperes and flow rates from less than 1 to about 18 gm/sec, argon. The corresponding values of $(J^2/\dot{m})$, tabulated in the last entry of table II, run from about 4 to about 80 $(KA)^2$ /gm, sec^{-1}. These values bracket the critical value of $(J^2/\dot{m})$ for argon, which is about 40 $(KA)^2/gm$, sec^{-1}.

The data in table II, although by no means complete, are quite interesting. They support certain trends, which are documented in figs. 16 and 17. In these figures, we plot electrode losses versus the important parameter $(J^2/\dot{m})$, for argon. Fig. 16 illustrates the fractional electrode losses. We see that at very low values of $(J^2/\dot{m})$, (low currents and/or high flow rates), each of the electrode losses is in the vicinity of 30 percent. Moreover, as $J^2/\dot{m}$ increases, we observe a moderate increase of the anode loss, while a moderate reduction is evident for the cathode loss. As a result of these trends, the total fractional loss shows, originally, a very modest decline and eventually levels at a plateau between 50 and 60 percent.

It is more informative to interpret the data in terms of equivalent anode and cathode falls. After applying relations (18) and (19), we plot the results in fig. 17, together with the MPD voltage corresponding

TABLE II

NUMERICAL EXAMPLES OF MPD ELECTRODE CALORIMETRY, IN ARGON

Average Losses are Established in the Steady State, from Long Runs of Repetitive Pulsing

	Number					
	1	2	3	4	5	6
$\dot{m}$, gm/sec	6	6	18	18	2	0.7
J, kiloamps	14	10	16	9	10	7.5
V, volts	83	70	72	67	120	165
JV, megawatts	1.16	0.70	1.15	0.60	1.2	1.24
Pulse Duration, millisec	1.3	1.4	1.3	1.5	1.4	1.5
Rep Rate, pps	0.5	0.5	0.5	0.5	0.5	0.5
Average Input, watts	750	500	750	450	840	930
Average Anode Loss, watts	250	166	225	144	280	340
Average Cathode Loss, watts	160	124	215	129	168	146
Average Total Loss, watts	410	290	440	273	448	486
Fract. Anode Loss, percent	33	33	30	32	33	37
Fract. Cathode Loss, percent	22	25	29	29	20	16
Fract. Total Loss, percent	55	58	59	62	53	52
Equiv. Anode Fall, volts	28	24	22	21	40	61
Equiv. Cathode Fall, volts	17	18	21	19	24	26
$(J^2/\dot{m})$, $(KA)^2$ /gm, sec^{-1}	33	17	14	4.5	50	80

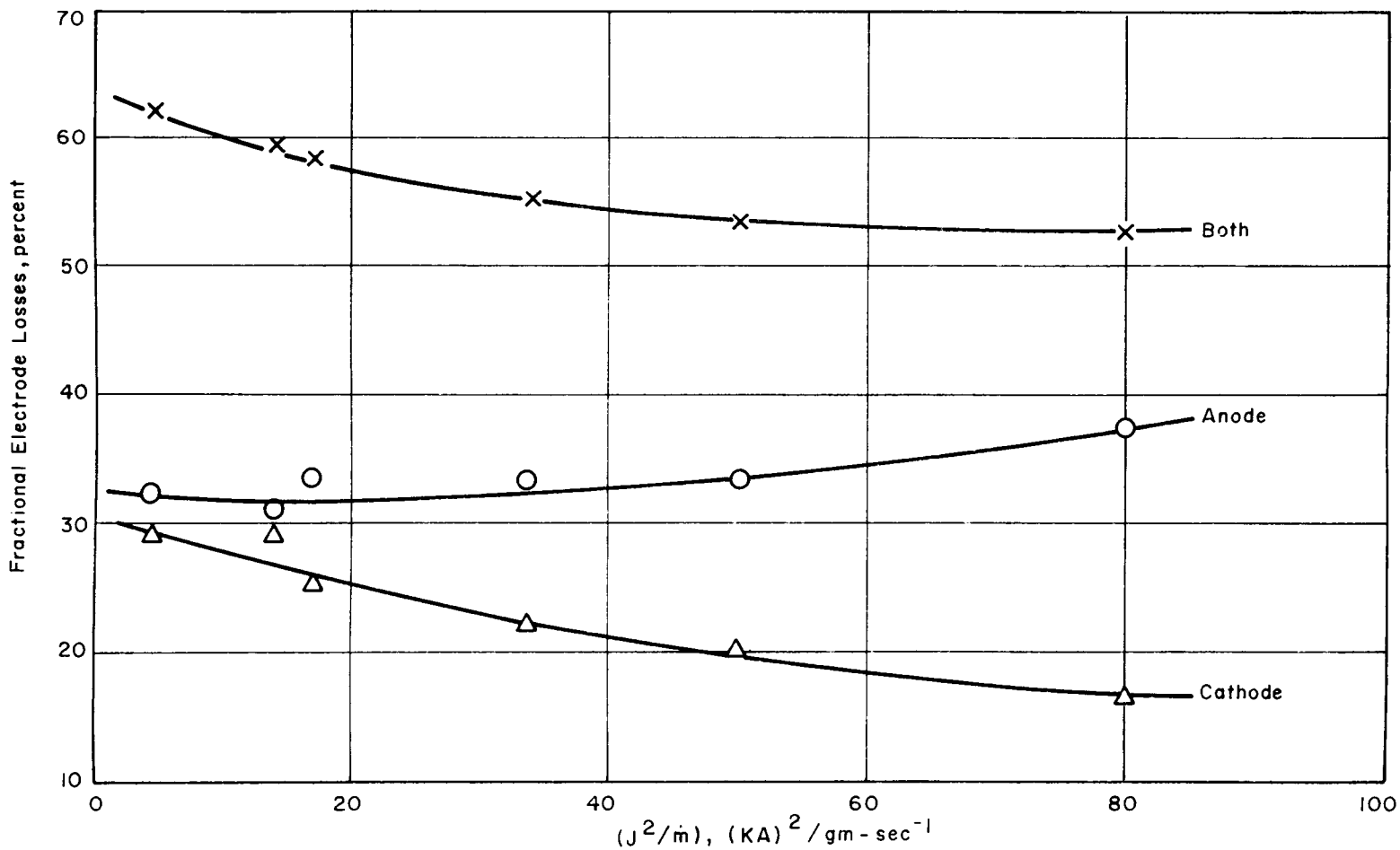

Figure 16 FRACTIONAL POWER LOSSES IN THE MPD ELECTRODES VERSUS $(J^2/\dot{m})$ FOR ARGON

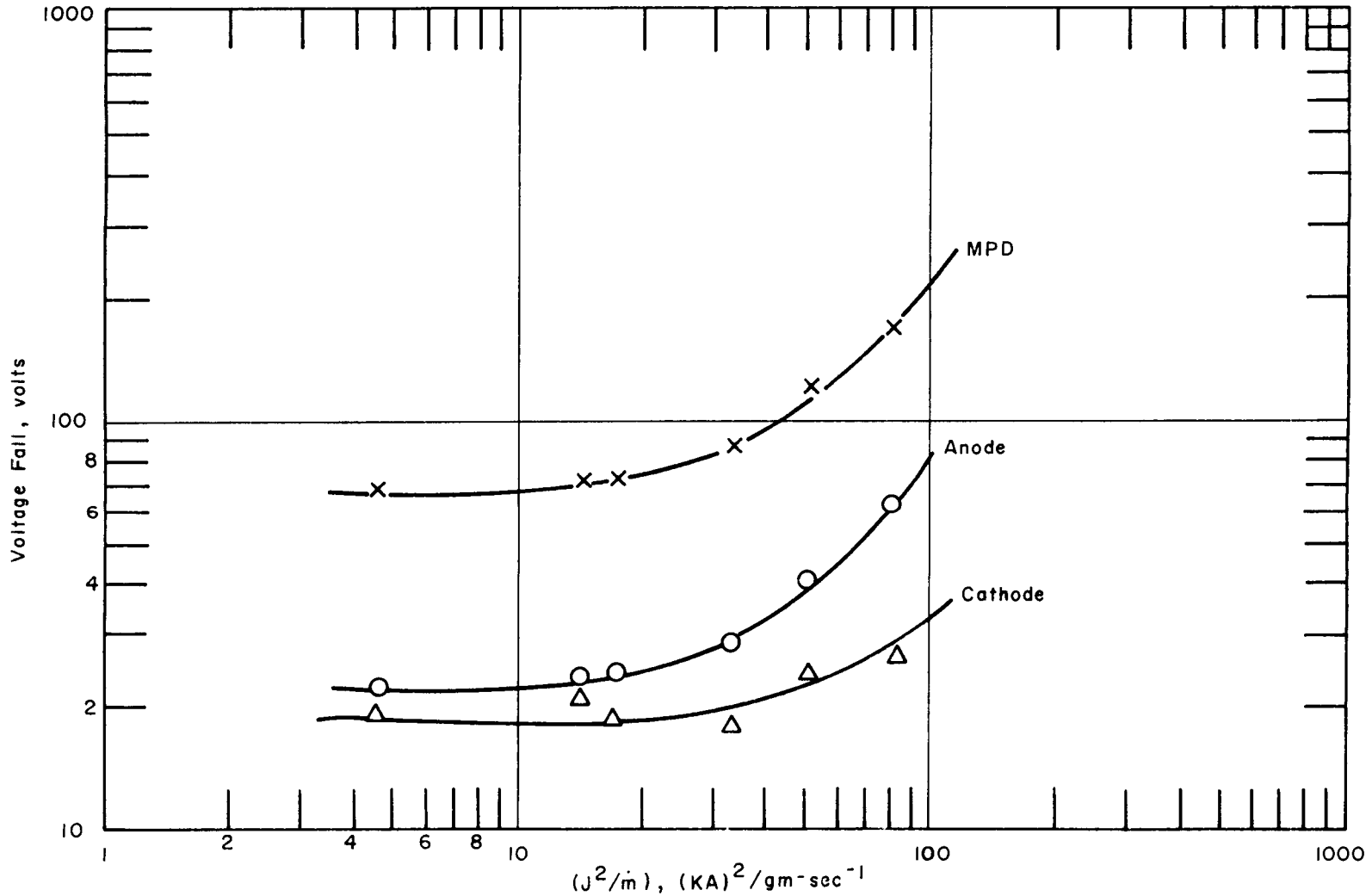

Figure 17 EQUIVALENT ELECTRODE FALLS AND MPD VOLTAGE VERSUS $(J^2/\dot{m})$ FOR ARGON

to each case. We easily note in fig. 17 that the MPD voltage rises sharply when the parameter $(J^2/\dot{m})$ exceeds a value about 40 $(KA)^2/gm$, sec^{-1}, believed to be the critical value for argon. However, it is very important to note that this rise in MPD voltage does not necessarily reflect a higher efficiency, since the equivalent anode and cathode falls also rise with a comparable sharpness. This behavior is naturally reflected in the fact that the fractional losses (see fig. 16) do not change appreciably.

In summary, our experimental evidence supports the conclusion that an argon, quasi-steady MPD operating around one megawatt has a total fractional loss about 55 percent. This is so regardless of the individual values of MPD current and flow rate, at least within the range indicated in table II.

It is also interesting to note that these trends are supported by independent evidence found in other laboratories, see refs. 6 and 9. This evidence, although indirect, is quite relevant since it deals with potential and current probing in the zones of cathode and anode potential falls.

V. MPD FLOW VELOCITY MEASUREMENTS

A. INTRODUCTORY REMARKS

As is well known, the specific impulse, I_{sp} , is a very important parameter of a high-power, quasi-steady MPD thruster. There are generally two experimental approaches in deriving an experimental estimate of the specific impulse. The first involves direct measurements of the impulse generated by the thruster when a certain amount of propellant is expelled under power. This will be examined and evaluated in the next section. The second method of specific impulse determination is less direct and involves measurements of the flow velocity at relevant stations of the MPD flow. These methods are complementary, in the sense that the first generally offers more directness and reliability, while the second offers more resolution and more information regarding non-uniformities, etc.

The MPD flow velocities are probed and determined in this program by Doppler-shift measurements of selected spectral lines emitted by the various species of the MPD propellant.

The general experimental arrangement for this type of work has been documented previously in refs. 10 and 11. Moreover, the particular arrangement and type of measurements for the quasi-steady MPD are described in ref. 5. In this section, we present experimental results which are relevant in the overall evaluation of the quasi-steady MPD thruster. The values of the specific impulse reported here are actually

flow velocity measurements which are converted into I_{sp} values, according to the detailed discussion given in ref. 5. In this reference also, we have included all the experimental evidence which concerns axial and radial profiles of the velocity in the MPD flow field.

Velocity determinations have been made for both ionic and neutral species. For identification purposes, the most prominent spectral lines, used in this task, are tabulated in table III.

TABLE III

MOST PROMINENT SPECTRAL LINES USED IN THE DOPPLER EXPERIMENTS

Propellant	Specie	Wavelength, A
Helium	Neutral	5875
	Neutral	4471
Neon	Ion	4392
	Neutral	5852
Argon	Ion	4806
	Ion	6644
	Neutral	6965
	Neutral	7067
Krypton	Ion	4659
	Neutral	5871
Xenon	Ion	4807
	Neutral	5460

B. RESULTS AND DISCUSSION

Experiments have been carried out for the determination of the flow velocity (specific impulse) at critical values of $(J^2/\dot{m})$, for

several gases. Specifically, the five noble gases were employed as propellants at mass flow rates and at MPD currents such that $(J^2/\dot{m})$ has the critical values determined previously and shown in fig. 13. Velocity determinations were made for both ionic and neutral species, but no detectable disparities were found in these velocities.

Furthermore, for two of the gases, namely argon and helium, velocity measurements were made at values of $J^2/\dot{m}$ both above and below the critical value. We proceed now to present and discuss our data:

1. Velocity Measurements and I_{sp} Determination at (J^2/m)

In one set of such experiments, the MPD current was kept constant at 20 kiloamperes for all propellants, but the mass flow rate of each propellant was adjusted according to the appropriate values of $(J^2/\dot{m})$, as given in figs. 13 or 14. In essence, we used about:

4.0 gm/sec of Helium

8.5 gm/sec of Neon

10.0 gm/sec of Argon

14.5 gm/sec of Krypton

21.0 gm/sec of Xenon

The experimental results are presented in fig. 18, where we plot the specific impulse (corresponding to the Doppler-determined velocities) versus the molecular weight of the propellant.

The similarity of the trends in figs. 13, 14 and 18 is quite striking. Evidently, the specific impulse of any propellant at the

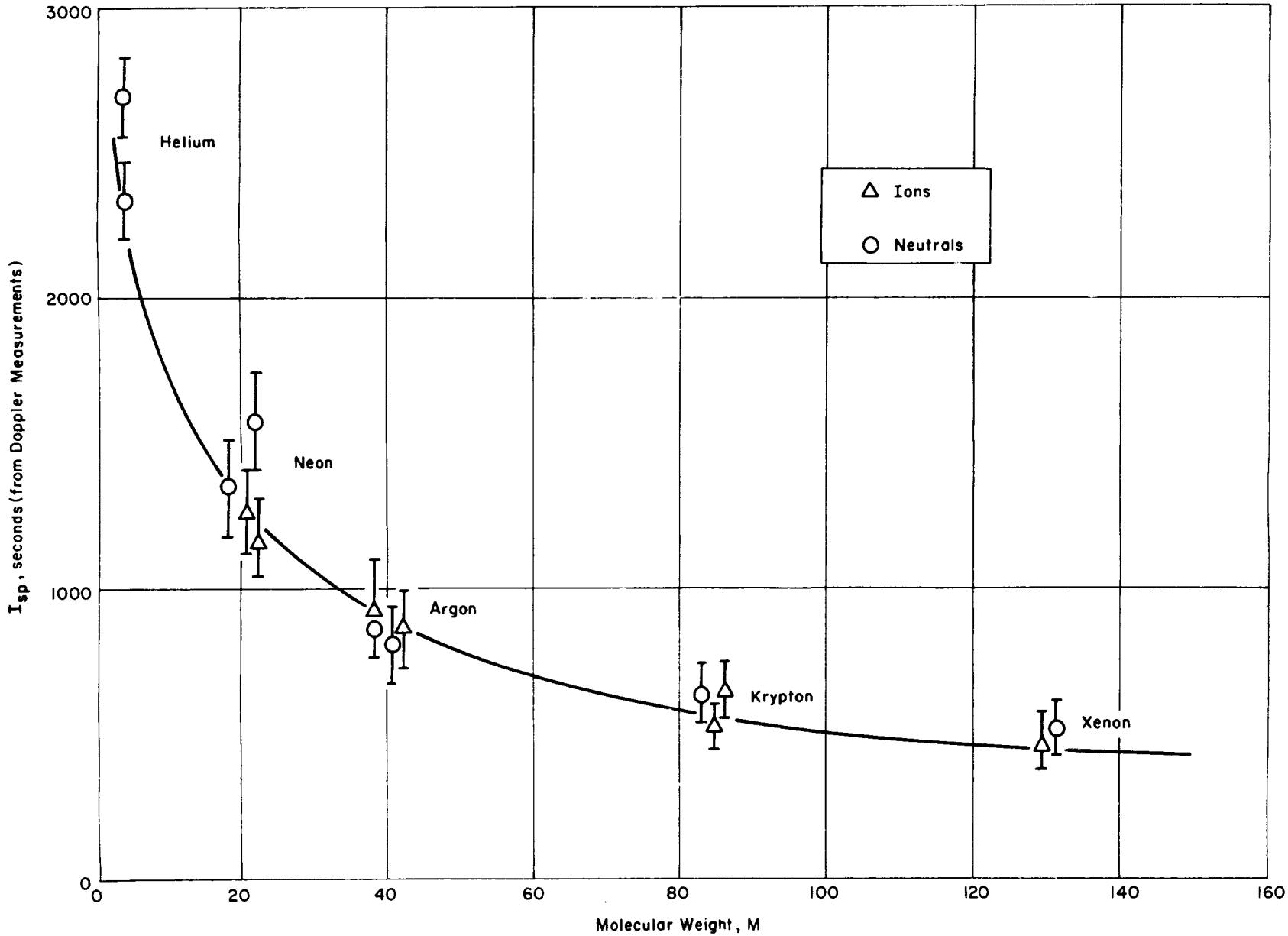

Figure 18 SPECIFIC IMPULSE FROM DOPPLER MEASUREMENTS VERSUS MOLECULAR WEIGHT AT CRITICAL ($J^2/\dot{m}$)

critical value of $(J^2/\dot{m})$ appears to be proportional to this value of $(J^2/\dot{m})$. This may be seen, more clearly, in the illustration of fig. 19, where we plot the specific impulse versus $(J^2/\dot{m})_{crit}$. In essence, this is a combination of the plots in figs. 13 and 18.

Next, we examined the question of the critical specific impulse as a function of the MPD current for a fixed propellant. Thus, for argon, we measured Doppler shifts and determined the flow velocities corresponding to five different currents, namely: 10, 15, 20, 25 and 30 kiloamperes. In these five cases we used, respectively, the argon flow rates of 2.5, 5.6, 10, 15.6 and 22.5 gm/sec. The values of the specific impulse resulting from Doppler measurements are tabulated in table IV.

TABLE IV

SPECIFIC IMPULSE AT CRITICAL $(J^2/\dot{m})$ FOR ARGON

J, kiloamperes	$\dot{m}$, gm/sec	$(J^2/\dot{m})$, $(KA)^2/gm, sec^{-1}$	I_{sp}, seconds
10	2.5	40	830
15	5.6	40	920
20	10.0	40	700
25	15.6	40	720
30	22.5	40	840

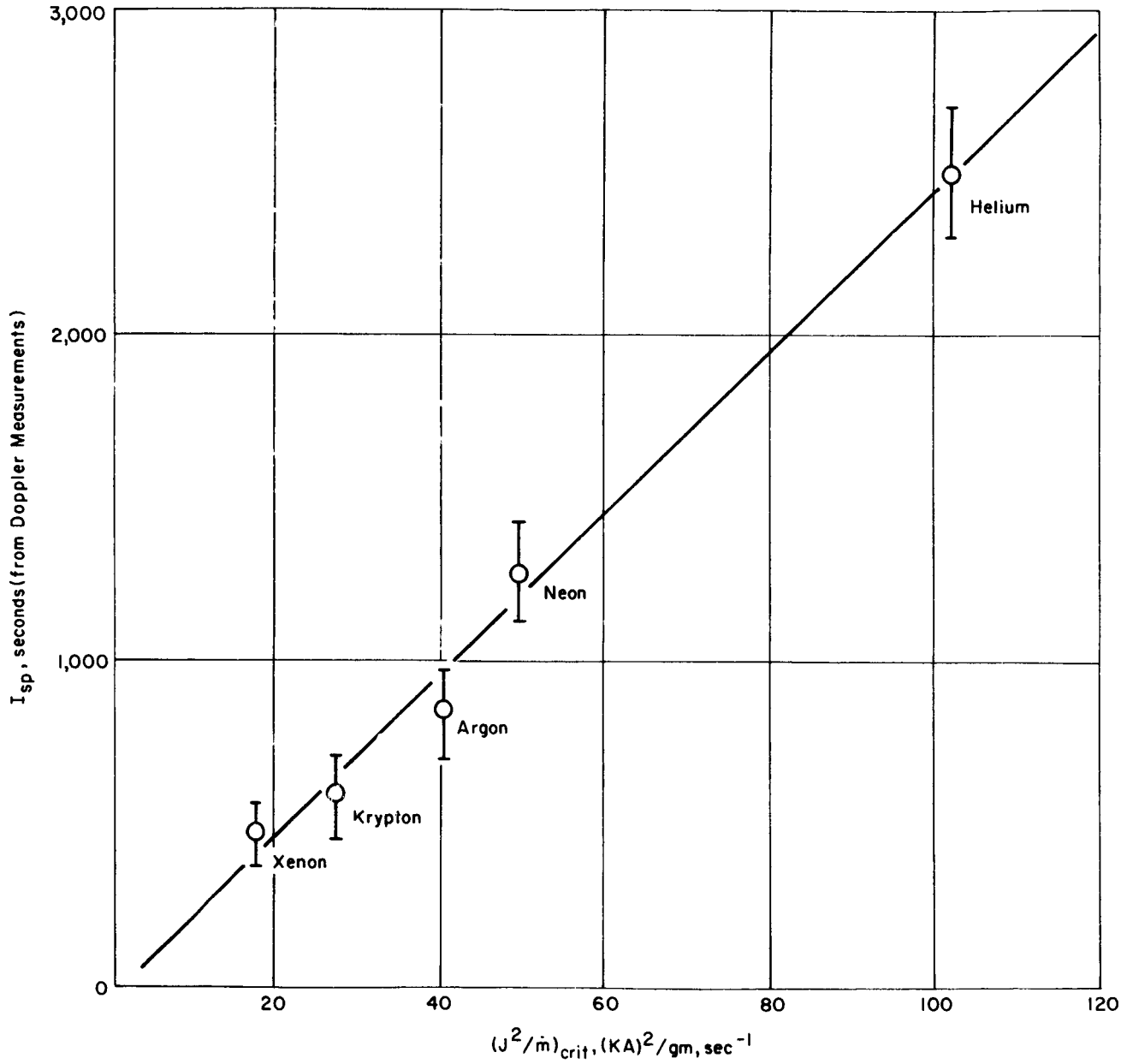

Figure 19 SPECIFIC IMPULSE FROM DOPPLER MEASUREMENTS VERSUS CRITICAL VALUES OF $(J^2/\dot{m})$ FOR SEVERAL PROPELLANTS

The straight average of these values of I_{sp} is about 800 seconds and the corresponding differences are +4, +15, -12, -10 and +5 percent, which are well contained within the experimental uncertainties.

Similar results have been obtained with helium as the propellant. Doppler measurements at 10, 20 and 30 kiloamperes and at appropriately matched flow rates [$(J^2/\dot{m})$, about 100 $(KA)^2/gm, sec^{-1}$] yielded a specific impulse of about 2400 seconds, in all three cases within ±10 percent.

2. Velocity Measurements and I_{sp} Determination at Values of $(J^2/\dot{m})$ other than Critical

This question has been examined mainly for argon at values of $(J^2/\dot{m})$ both below and above the critical. A large variety of current and flow rate combinations has been used here, in the ranges 7 to 30 kiloamperes and 0.5 to 25.0 gm/sec, argon. The corresponding range of $(J^2/\dot{m})$ values has been from 10 to about 300 $(KA)^2/gm, sec^{-1}$. As is the case for the data presented in the previous subsection, there is no substantial difference in the values of I_{sp} determined at a given value of $(J^2/\dot{m})$, regardless of the individual values of J and $\dot{m}$. For this reason, we present these data in a general fashion as I_{sp} versus $(J^2/\dot{m})$. This is done in fig. 20.

It is clear in this figure that a specific impulse between 800 and 900 seconds corresponds to the critical value of about 40 $(KA)^2/gm, sec^{-1}$ for argon. This result has been discussed in

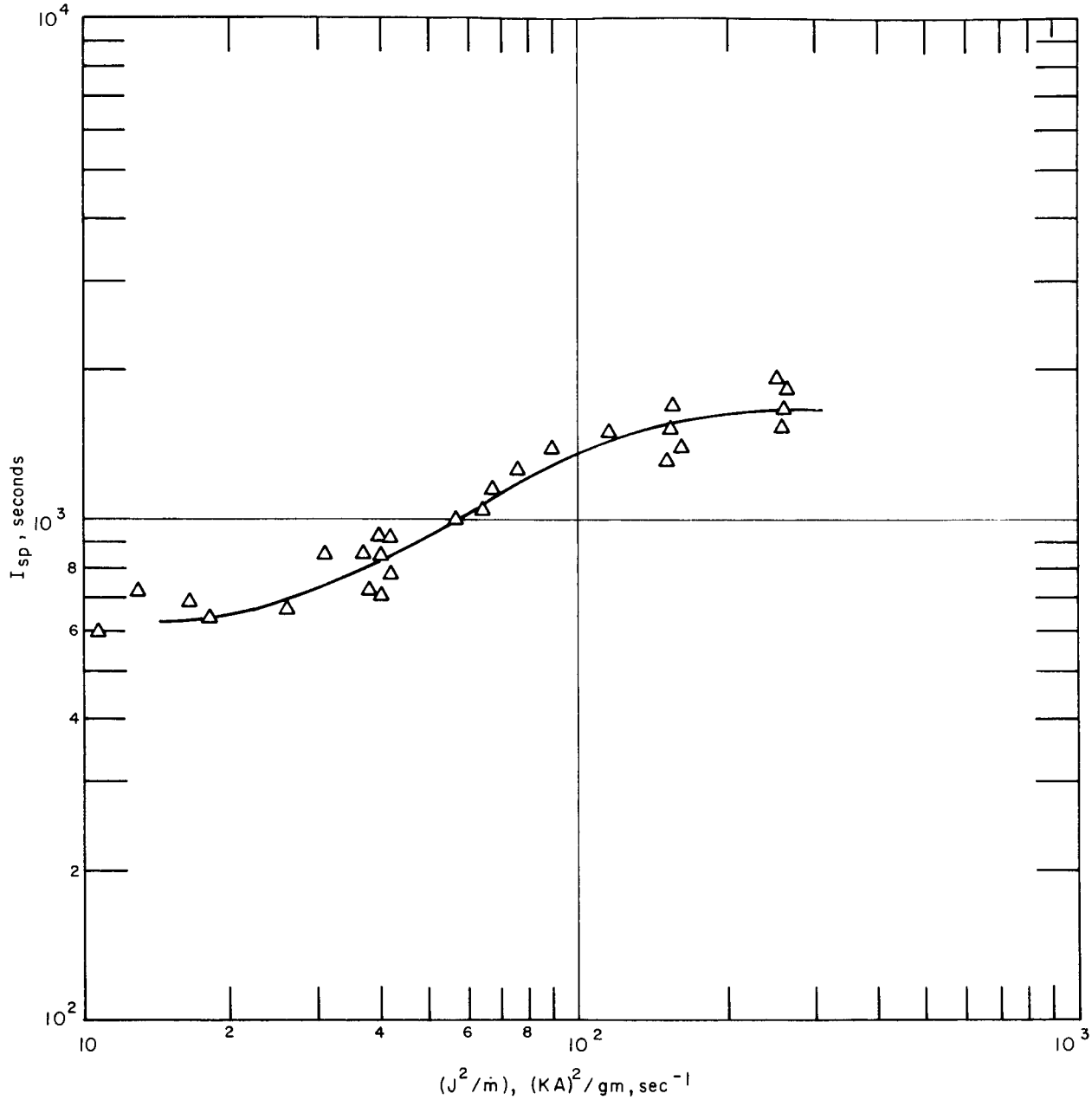

Figure 20 SPECIFIC IMPULSE FROM DOPPLER MEASUREMENTS VERSUS THE PARAMETER $(J^2/\dot{m})$ FOR ARGON

the previous subsection and is in fair agreement with the analytical expectation for argon:

$$(I_{sp})_{crit} = (T/\dot{m})_{crit} = b(J^2/\dot{m})_{crit}$$

As noted earlier in the discussion following Eq. (6), the value of b for our accelerator is about 2×10^{-7} MKS.

The results of fig. 20, however, are quite important in demonstrating the behavior of the Doppler measured specific impulse at values of $(J^2/\dot{m})$ both higher and lower than the critical value. In the absence of any evidence regarding critical values, we would expect, generally, the specific impulse to increase linearly with $(J^2/\dot{m})$. Clearly, this is not supported by the experimental data of fig. 20. As the value of $(J^2/\dot{m})$ increases beyond the critical value of 40, we see that I_{sp} increases only marginally, and gradually it reaches a plateau. This behavior, plus more additional evidence, is a strong indication of I_{sp} limitations, which may not be uncovered from direct impulse measurements. As recalled, this range of conditions has been designated as the MPD starvation region.

Similar observations can be made in the range of $(J^2/\dot{m})$ values, below the critical. This is the so called "overfed" MPD region. Here normally, we would expect the I_{sp} values to decrease in proportion to the decreasing $(J^2/\dot{m})$ values. However, this is not observed with the flow velocities (converted into I_{sp}) of fig. 20. These

data must eventually be discredited, since at sufficiently low values of $(J^2/\dot{m})$, the energy conservation principle is violated. Several examples may be found at our laboratory and elsewhere (see ref. 3), where the kinetic power of the MPD $(\dot{m} I^2_{sp}/2)$ exceeds the total input power. Evidently in the overfed MPD region, it appears that only a fraction of the fed $\dot{m}$ is substantially accelerated, while the balance of the propellant is not participating. This seems to be a reasonable alternative to the aforementioned discrepancies. It will be quite interesting to compare the data of fig. 20 with I_{sp} values derived from impulse measurements under the same experimental conditions.

VI. IMPULSE MEASUREMENTS

It is very essential, in programs of the type under consideration here, to make measurements of the impulse resulting from a quasi-steady MPD thruster. For this purpose, we have carefully evaluated the possibility of such measurements. In the following two sections, we demonstrate how such measurements may be made with reliability, and we present some illustrative results.

A. THE MEASUREMENT OF IMPULSE BITS

For these measurements, we have modified appropriately a facility developed at Avco under program NAS-5-10342. In this facility, the thrust* and/or impulse measuring device is essentially a mass-balanced, single-axis suspended table, where the impulse to be measured is normal to, but does not pass through, the axis of rotation. Specifically, the MPD impulse, acting at a known moment arm, produces an angular velocity of the suspended table, which is very accurately measured with a rate gyro also mounted on the table. Thus, the relevant relations are:

$$H = Q \cdot \dot{w} \tag{20}$$

*Strictly speaking, no thrust measurements can be made with submillisecond resolution. Thus, although the average thrust from repetitive pulsing can be determined easily, the instantaneous thrust, during a single MPD pulse, can not be resolved. Instead, the time integral of this thrust, over the pulse duration, is accurately determined.

where $\dot{w}$ is the measured angular velocity of the table, Q is its calibrated rotational inertia, and H is the angular momentum resulting from the MPD impulse bit, I_b , as follows:

$$H = s \cdot I_b \tag{21}$$

with s representing the known moment arm of the MPD.

In the above relations, we have assumed that the suspended table is truly inertial in the angular sense. This, in essence, means that the table is free of torques, other than the one produced by the MPD thrust. In fact, the inertial table is free of parasitic torques, and thus it has zero, parasitic, angular acceleration, not only during the pulse but also for arbitrarily long periods, either before or after the MPD impulse. Thus, when a certain angular momentum is determined by Eq. (20), it may be associated directly to the MPD impulse bit, see Eq. (21), no matter how long it takes to make this determination.

Zero parasitic torques and angular acceleration are naturally mathematical conveniences. In our laboratory practice, any possible parasitic* torques and accelerations may arise mainly from the twist of the suspension wire. If at any time the twist angle of the suspension

*We are talking here exclusively about parasitic torques of purely mechanical origin. The question of parasitic torques of purely electromagnetic origin (interaction of currents on the inertial table with tank walls or other structures, etc.) does not enter at all into the design of the inertial table. This question has been answered directly and separately by a comparison of normal MPD impulse measurements with similar measurements under thrust killing arrangements. This comparison has shown that parasitic effects of this nature are of the order of 1 percent or smaller.

wire is w^*, then a parasitic (restoring) torque exists, which is given by:

$$L^* = k \cdot w^* \tag{22}$$

where k is the wire constant for torsional oscillations.

Accordingly, the table will be considered truly inertial for all practical purposes if the integral of $L^* dt$ is negligibly small, not simply over the MPD pulse duration, but over any duration, t^*, required for the angular velocity measurement. The integral under consideration is the parasitic angular momentum:

$$H^* = \int_o^{t^*} L^* dt \tag{23}$$

which may falsify the angular momentum, H, associated with the MPD impulse bit.

We may derive a good estimate of the falsifying effect as follows: Let an angular momentum, H, be generated by the MPD impulse. According to Eq. (20) we have:

$$(dw^*/dt) = (H/Q) \tag{24}$$

where we have used the asterisk to designate the twist angle of the wire. Thus, in the first approximation, i.e., in the absence of a substantial restoring torque, we may write:

$$w^* = (H/Q)\, t \tag{25}$$

assuming that the twist angle is zero at t=0. With this approximate time dependence of the twist angle, we proceed to estimate the parasitic torque from Eq. (22), and then the parasitic angular momentum from Eq. (23). Integrating from zero to any desirable time, t^*, (arbitrarily longer than the MPD pulse duration) we obtain:

$$H^* = (Hk/2Q)(t^*)^2 \tag{26}$$

Thus, the relative disturbance of the parasitic angular momentum is given by:

$$(H^*/H) = 2\eta^2 (t^*/T_{tors.})^2 \tag{27}$$

where we have taken into account that the period of torsional oscillations is given by:

$$T_{tors.} = 2\eta (Q/k)^{1/2} \tag{28}$$

It is obvious in Eq. (27) that the relative disturbance will be negligible if the period of torsional oscillations is much longer than the time interval, t^*, necessary for the angular velocity determination. Moreover, as suggested by Eq. (28), the torsional period may be extended by arranging so that the inertial table has a sufficiently large, Q, rotational inertia, and so that the suspension wire has a constant k as small as possible.

In our laboratory practice, the rotational inertia may not be made arbitrarily large. In other words, there are limitations on both the total suspended mass and on the deployment of this mass in the radial sense. Besides, an arbitrarily large Q would seriously limit the minimum angular momentum (and thus minimum MPD impulse) that may be measured,

even with a very sensitive gyro. (See Eq. (20).) As will be explained shortly, we find that a rotational inertia of 10 to 20 slug-ft^2 (or 1.4×10^8 to 2.8×10^8 cgs) is both convenient and adequate for our experiments. For example, the inertial table in typical experiments, reported in the Appendix, has a rotational inertia of about 1.8×10^8 cgs. This includes the thruster, capacitor bank, propellant supply tank, pulsed valve and the auxiliary gadgetry, all onboard the table. Incidentally, the total mass of this system is a few hundred pounds, which is well within the 800-pound weight limitation imposed by the finite strength of the suspension wire.

In pulsed MPD experiments, the impulse bit is generally expected to be in the range 1 to 100 mlb-sec (or 5×10^2 to 5×10^4 cgs). Moreover, in our case the moment arm of the MPD is about 2 feet (or 60 cgs). Accordingly, the resulting angular momenta, see Eq. (21), are in the range 3×10^4 to 3×10^6 cgs. With the mentioned rotational inertia of 1.8×10^8 cgs, the resulting angular velocities, see Eq. (20), are in the range 1.7×10^{-4} to 1.7×10^{-2} radians/sec, or about 0.01 to 1 deg/sec. This is quite an agreeable range for the rate gyro, from the viewpoints of sensitivity, linearity, etc. At a sensitivity of about 540 millivolts per deg/sec, the said gyro, in the said range, provides a linear signal between 5.4 and 540 millivolts, which is quite adequate for detection and recording.

Regarding now the suspension wire, we remark the following: The suspension of the inertial table is not made through a single wire of a given cross-section, but through a large number of closely spaced wires with a much smaller cross-section. This arrangement obviously allows the suspension to have a large weight capacity and at the same time it results in a relatively low value of the torsional constant, k. Presently, this constant has a value about 3×10^4 cgs. At the mentioned value, 1.8×10^8 cgs for the rotational inertia, we obtain from Eq. (28) a period of about 500 seconds for torsional oscillations. Now note that, under any circumstances, an interval of say $t^* = 5$ seconds is quite adequate for detecting and recording an angular velocity due to an MPD impulse. It follows from Eq. (27) that, under such conditions, the relative parasitic angular momentum (due to the restoring torque) equals about 0.2 percent. Alternatively, this means that the angular velocity we try to measure for the MPD impulse determination will have a maximum error of about 0.2 percent if it takes as long as 5 seconds after the MPD impulse to determine the angular velocity of the inertial table. In actual practice of course, 5 seconds is quite adequate. In fact theoretically the gyro output may be displayed and recorded within milliseconds after the MPD impulse.

The analysis presented, in connection with the parasitic angular momentum and its effect on the MPD impulse determination, is naturally valid for relatively small values of the twist angle, w^*. In other words, the assumption is made that the MPD impulse is applied when the

suspended table is at or near the torsional equilibrium point. This, however, is not always the case, or at least not at any arbitrary time we wish to apply an MPD impulse.

We wish to point out here that up to now the suspended table is not yet an inertial table but simply a torsional pendulum which approximates fairly close an inertial table. The approximation is good only for positions and times near the equilibrium point, at which point the table has a relatively small acceleration. As explained in the discussion above, the approximation is good to 0.2 percent for times up to 5 seconds before or after the equilibrium point, and varies as the square of this time, see Eq. (27), provided that the said time remains always much smaller than T_{tors}, which is about 500 seconds.

An additional convenience, incorporated in our facility, makes the suspended table an inertial table to an excellent approximation, regardless of any particular time or length of time. This is accomplished by making the twist angle, w^*, of the suspension wire negligibly small, at all times, regardless of the angular displacement of the suspended table, with respect to a laboratory frame of reference.

In our laboratory practice, this is realized by suspending the table not directly from the tank ceiling, but from a platform. A servo, torque-motor mechanism slaves the platform to the suspended table so that the twist angle of the suspension wire is and remains negligibly small, regardless of the angular position or the angular velocity of

the suspended table. The coupling between the upper platform and the suspended table is accomplished by means of a polarized and well collimated light beam, generated on the suspended table and sensed on the platform.

Under these conditions, the test table under consideration becomes rotationally inertial, i.e., free of parasitic torques, within an uncertainty of $\pm 10^{-6}$ ft-lbs, or about 13.5 cgs. This is negligible for all practical purposes.

In the experiments under consideration here, the environmental tank, 6-feet diameter 8-feet long, is evacuated by a large diffusion pump, down to pressures of the order of 10^{-3} microns Hg. Furthermore, the rate-gyro output is continuously recorded versus time, so at any instant we may easily measure any angular velocity and acceleration, as well as any discontinuity of the angular velocity associated with an MPD impulse.

Finally, the rotational inertia of the inertial table is calibrated by well established laboratory procedures. In practice, two approaches may be used: either a well known torque is applied and the resulting angular acceleration is measured, or a well known angular momentum is applied and the change in angular velocity is measured.

B. ILLUSTRATIVE EXAMPLES OF IMPULSE MEASUREMENTS

The facility described in the last section has been employed for impulse bit measurements of the quasi-steady, pulsed MPD system described in Section II-D. Some preliminary results are available for illustration purposes and are reported here in fig. 21. We have used two largely different values of $\dot{m}$ for argon, and power pulses with amplitudes up to several megawatts and durations in the range of 1 to 2 milliseconds.

The data in fig. 21 are plotted as directly measured impulse bits versus the corresponding integral of the MPD current waveform squared. The purpose is to compare the measured impulses with the analytically expected impulses, according to the self-magnetic origin of the thrust. The analytical expectation is presented as the solid straight line in fig. 21, and for reference we have used r_A = 3 inches and r_C = 3/4 inch.

It is fairly evident that at sufficiently high values of the J^2 integral, the impulse measurements are in good agreement with the analytical expectation. A deviation from the analytical expectation is observed as the integral of J^2 is reduced. Moreover, the observed deviations are much larger for the higher flow rates. Evidently, the discrepancy here may be easily accounted for by the so called electrothermal or gasdynamic contribution.

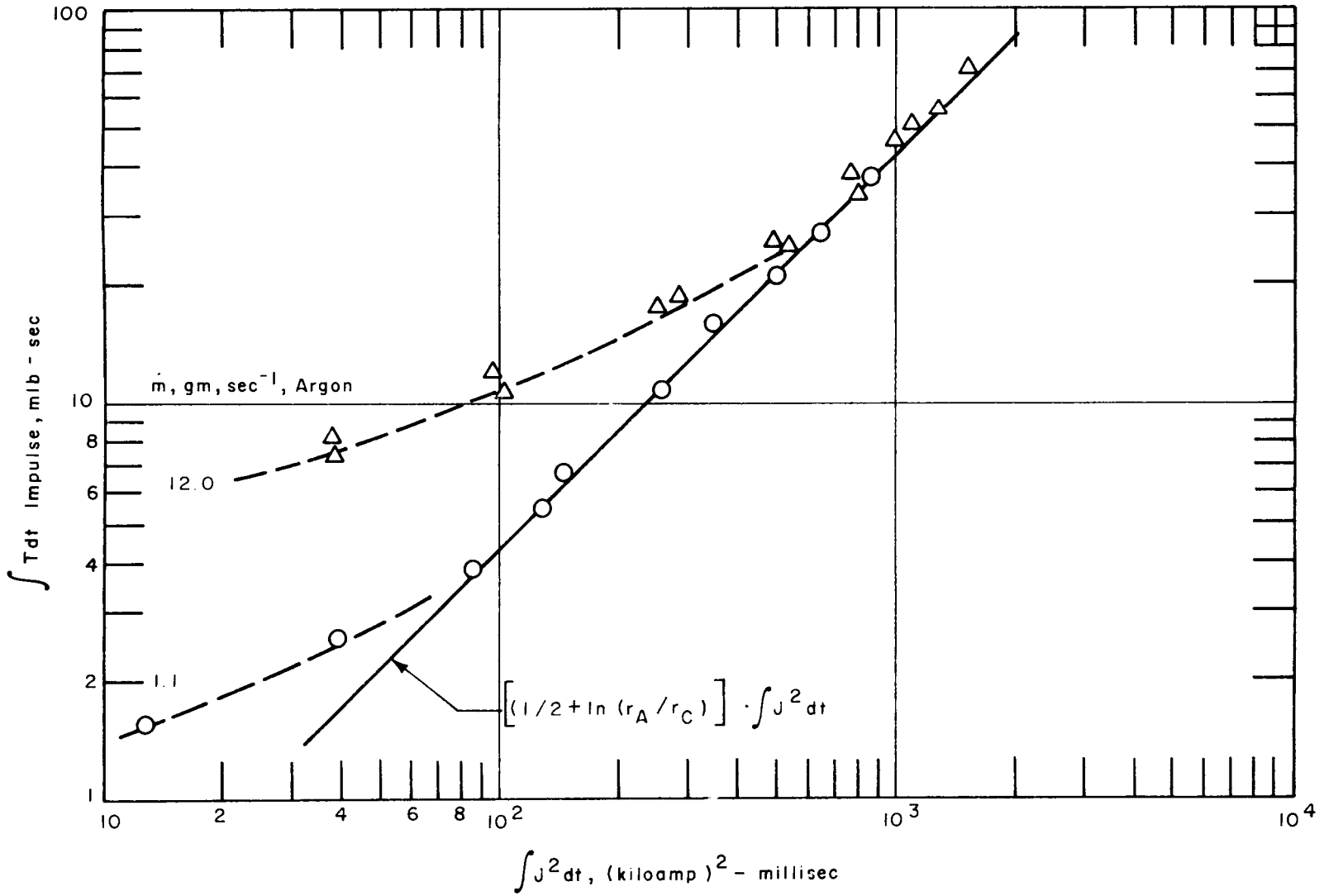

Figure 21 MEASURED IMPULSE BIT VERSUS MEASURED $\int J^2\,dt$ FOR ARGON

VII. SUPPORT SUBSYSTEMS

It is understood that a quasi-steady pulsed MPD thruster used in a pulsed plasma propulsion system requires special support in several ways, most importantly: (a) need for energy storage in a capacitor bank; (b) power processing for an efficient charging of capacitors, at a given constant power; and (c) An elaborate propellant feed system.

A fairly extensive task in this program deals with the determination of the qualifications of commercially available capacitors for use in pulsed MPD propulsion system. In essence, commercially available capacitors have been selected, tested and evaluated at our laboratory. This work is discussed in the Appendix, where we describe the type of capacitors selected for evaluation, the procedure followed in the evaluation, a series of laboratory tests and the final results.

The energy per pulse, stored in the capacitor bank of a pulsed MPD propulsion system, is provided by an average power supply, at a given voltage and power level. A power transformation is necessary, and this is not a trivial problem, if high efficiencies and low specific weights are desired. However, recent advances in power conversion, see for example ref. 12, justify the conclusion that this problem is under control, compared to other problems of a pulsed MPD system.

It appears that power converters, for applications of our interest here, are available, ref. 12, in the multi-kilowatt range, at specific weights about 5 lb/kw and efficiencies about 95 percent.

We now make a few remarks regarding the propellant feed system. First, we remark that in a repetitively pulsed, plasma propulsion system certain valveless concepts of propellant feed appear to have advantages of simplicity and reliability, over more conventional concepts, utilizing a repetitive valve and a gaseous propellant.

These advantages, demonstrated for example in microthruster systems, are clearly realized under the following conditions: (a) the total propellant for the mission is of the order of a few pounds, so that very simple and reliable feeding mechanisms are possible, (b) the amount of propellant per pulse is of the order of one micropound, and (c) pulse durations of the order of 10 microseconds are of interest. With such short pulse durations, the use of a valve is very questionable.

However, we are very skeptical about these conditions, regarding the case of the pulsed MPD, especially for primary propulsion applications. For example, in this case the total propellant requirement is at least 2 to 3 orders of magnitude higher than in the case of microthruster systems. Thus, with several hundred pounds of propellant, the extreme simplicity and versatility of the feed system is not applicable any more.

Similarly, we may object against the relevance of conditions (b) and (c) mentioned above. In other words, we feel they are too restrictive for a quasi-steady, pulsed MPD.

Finally, we remark that it would be premature to examine in detail any definite concept of propellant feed, in view of the increasing evidence, see figs. 15 and 18, that the molecular weight of the propellant is a rather strong parameter of the quasi-steady MPD performance. In this sense, the selection of the propellant, and consequently of the propellant feed, should await more final and definite conclusions about the role of the propellant in MPD performance.

VIII. CONCLUSIONS

In the following paragraphs, we review and summarize the conclusions reached in our investigation, regarding a high-power, quasi-steady MPD thruster and the associated system.

(a) Increasing evidence, at this and other laboratories, strongly suggests that this type of MPD thruster is subject to limitations in the choice of the current and flow rate. Specifically, there appears to be a critical value of $(J^2/\dot{m})$, above which the operation of the MPD thruster becomes increasingly erratic. In this range also, it becomes increasingly difficult to conserve energy and momentum balance in the MPD flow, unless an additional flow rate of propellant is allowed by ingestion of eroded and/or environmental material.

(b) It is equally important to note that the critical value of $(J^2/\dot{m})$ is a fairly sensitive function of the propellant properties. Specifically, it varies as the inverse square root of the molecular weight, see figs. 13, 14 and 15. The implication here is that heavy propellants should not be favored, since they are burdened with a very small value of $(J^2/\dot{m})$ and thus at any given current, a rather large value of $\dot{m}$ is required for acceptable operation.

(c) The specific impulse, as determined from Doppler-velocity measurements, appears to be a function of $(J^2/\dot{m})$ but does not depend substantially on the individual values of either J or $\dot{m}$. Moreover when $(J^2/\dot{m})$ increases beyond the critical value, the specific impulse appears to increase only marginally and eventually reaches a plateau.

(d) It is very important, from the practical point of view, to note that at the critical values of $(J^2/\dot{m})$ the available specific impulse increases linearly with $(J^2/\dot{m})_{crit}$, (See fig. 19.) This has the same practical implications as item (b) discussed above.

(e) A lower limit has been established for the losses in the operation of the pulsed MPD thruster. Results from MPD electrode calorimetry have shown that electrode losses account for 50 to 60 percent of the electrical power input when the accelerator is operated in the vicinity of one megawatt with pulse durations in the vicinity of one millisecond.

(f) The aforementioned result appears not to be very sensitive to $(J^2/\dot{m})$ for values either below or above the critical. In essence, the MPD voltage increases very sharply when $(J^2/\dot{m})_{crit}$ is exceeded, but it has been observed that both the anode and cathode equivalent voltage falls increase sharply also.

(g) It has been possible to make preliminary measurements of single impulse bits. These measurements show that, at sufficiently high values of the MPD current, the impulse results mainly from self-magnetic acceleration, see fig. 21, and is well accounted for by the square of the current and the MPD geometry. Substantial contributions of gasdynamic origin are evident at lower values of the current and especially for the higher flow rates.

(h) From the aforementioned preliminary data, it has been possible to derive values for the specific impulse. These values depend linearly on $(J^2/\dot{m})$ and are not sensitive to the individual values of J and $\dot{m}$, provided that the MPD current is sufficiently high. These data are summarized in fig. 22, where we compare them with the specific impulse values derived from Doppler-velocity measurements. It is interesting to note that over a range of $(J^2/\dot{m})$ from about 30 to about 60 $(KA)^2/gm, sec^{-1}$ of argon, the specific impulse values (about 700 to 1000 seconds) are the same in both methods. However, as $(J^2/\dot{m})$ increases beyond the aforementioned values, the specific impulse from impulse measurements keeps increasing, and this is not reflected in the corresponding velocity measurements. This resolves the unacceptable situations which arise when I_{sp} (determined from impulse measurements) keeps increasing

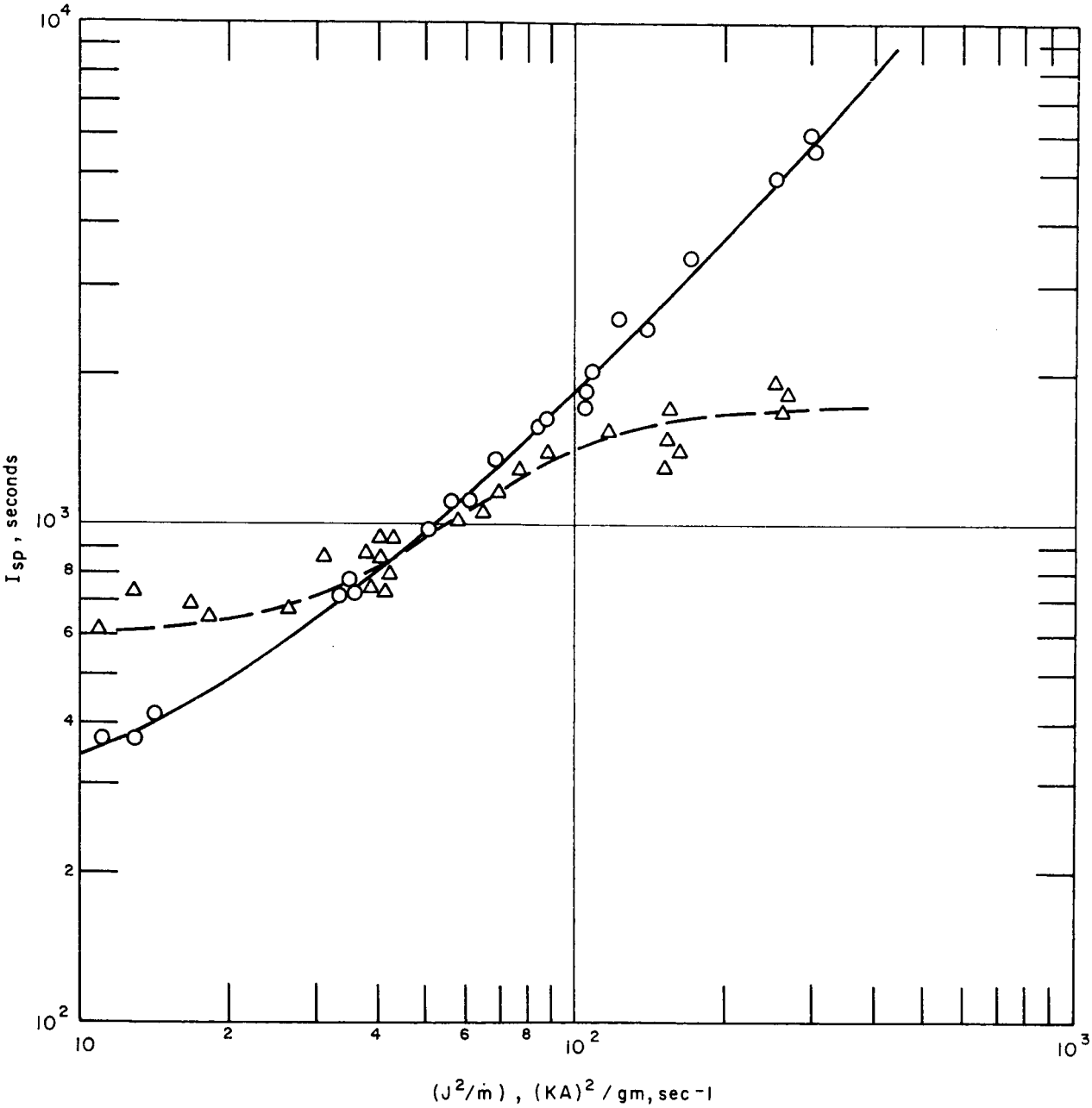

Figure 22 SPECIFIC IMPULSE VERSUS $(J^2/\dot{m})$.
Comparison of Velocity Measurements
(Triangles) with Preliminary Impulse
Measurements (Circles) for Argon

without apparent limit. Note that a similar trend has been observed in ref. 4.

(i) Further reference to fig. 22 shows that as $(J^2/\dot{m})$ is decreased below its critical value, the values of I_{sp} from velocity measurements fail to decrease proportionately, and this is not reflected in the impulse measurements. Evidently, such a disagreement would arise if, under these "overfeeding" conditions, only a fraction of the fed $\dot{m}$ is accelerated, while the rest of the propellant is not participating substantially.

Two more conclusions of practical importance are included here:

(j) Although it is not the purpose of this work to establish the life-expectancy of an MPD thruster, we did find that no serious problems were encountered with the structural integrity of the particular thruster employed in our experiments. This is based on a total number of pulses as high as 10,000, delivered either singly or repetitively, at rates of the order of 1 pps. Typical powers in the range 1 to 10 megawatts and typical durations of the order of 1 millisecond are relevant.

(k) The ohmic impedance in the system from the capacitor bank to the MPD amounts to about 2.5 milliohms, excluding the MPD. If a typical MPD impedance as high as 7.5 milliohms is

considered, we see that the losses (other than MPD thruster losses) amount to about 25 percent. This fraction is large, in spite of the fact that every effort was made to minimize the ohmic impedance (regardless of weight and size penalties) of all components such as PFN capacitors and inductors, switches, transformer windings, power leads, etc. The implication here is that it will be difficult to keep these parasitic losses lower than 25 percent in a high-power, pulsed MPD propulsion system, especially if serious limitations are imposed on the weight and size of the system.

REFERENCES

1. Malliaris, A. C., D. R. Libby and R. R. John: "High Power Quasi-Steady MPD Acceleration," NASA Technical Report, NASA CR-111785, May 1970.
2. Clark, K. E. and R. G. Jahn: "Quasi-Steady Plasma Acceleration," AIAA Paper 69-267, 1969.
3. Jahn, R. G., et al.: "Acceleration Patterns in Quasi-Steady MPD Arcs," AIAA Paper 70-165, 1970.
4. Hoell, J. M., J. Burlock and O. Jarrett, Jr.: "Velocity and Thrust Measurements in a Quasi-Steady Magnetoplasmadynamic Thruster," AIAA Paper 70-1080, 1970.
5. Malliaris, A. E. and R. R. John: "Outstanding Problems Regarding the Feasibility of a Repetitively Pulsed MPD Accelerator," AIAA Paper 70-1093, 1970.
6. Turchi, P. J. and R. G. Jahn: "The Cathode Region of a Quasi-Steady MPD Arcjet," AIAA Paper 70-1094, 1970.
7. Clark, K. E. and R. G. Jahn: "Quasi-Steady Plasma Acceleration," NASA NGL 31-001-005. Aerospace and Mechanical Sciences Report No. 859, May 1969, Princeton University, Princeton, N. J.
8. DiCapua, M. S. and R. G. Jahn: "Energy Deposition in Parallel Plate Plasma Accelerators," AIAA Paper 71-197, 1971.
9. Oberth, R. C. and R. G. Jahn: "Anode Phenomena in High-Current Accelerators," AIAA Paper 71-198, 1971.

10. Malliaris, A. C. and D. R. Libby: "Velocities of Neutral and Ionic Species in an MPD Flow," AIAA Paper 69-109, 1969.

11. Malliaris, A. C. and D. R. Libby: "Spectroscopic Study of Ion-Neutral Coupling in Plasma Acceleration," AIAA Paper 70-166, 1970. Also to be published in AIAA Journal.

12. Schwarz, F. C.: "A Method of Resonant Current Pulse Modulation for Power Converters," IEEE Transations on Industrial Electronics and Control Instrumentation, Vol. IECI-17, No. 3, May 1970, pp. 209-221.

APPENDIX

TESTS AND EVALUATION OF COMMERCIALLY AVAILABLE CAPACITORS

First, we outline the general guidelines for considering and selecting certain types of capacitors. In essence, we are looking for energy storage, pulse-discharge duty capacitors. A slow charge period, to voltages between few hundred and few thousand volts, should be followed by a fast discharge, with a waveform as rectangular as possible. For the applications we have in mind, the discharge duration is of the order of a millisecond, while duty cycles about 10^{-3} are relevant. In other words, rep rates in the range 1 to 10 pps are relevant.

Furthermore, it appears reasonable to make the assumption that voltage reversals will be kept within 20 percent or lower, since the capacitors under consideration would be used in pulse forming networks with an impedance closely matched to the load.

With the aforementioned guidelines in mind, we have proceeded to evaluate the two most important qualifications of commercially available capacitors, namely:

Energy losses per charge-discharge cycle, or alternatively, power losses in repetitive operation, and

Energy density or specific weight.

A. CAPACITOR TYPES

From the presently available capacitors, we have considered three general types:

Type (a): Relatively modern capacitors for energy storage and pulse discharge duty. The dielectric in these capacitors is, usually, thin plastic film plus low viscosity oil. Extended foil construction is employed.

Type (b): Relatively older types of energy storage capacitors, with oil impregnated paper dielectric, and no extended foil construction.

Type (c): Modern electrolytic capacitors with ratings in the vicinity of 1000 microfarads, 400 volts. Electrolytic capacitors are generally not qualified for energy storage and pulse discharge duty. However, we include them here for comparison purposes, especially since several investigators seriously consider the application of such capacitors.

In the evaluation, we considered first the technical literature and engineering bulletins of reputable manufacturers such as: General Electric, Maxwell Laboratories, Sprague, Cornell-Dubilier, Aerovox, Mallory and others. Following a preliminary screening, we attempted to clarify several points by direct consultation with the manufacturers. The results were only partially satisfactory, especially regarding the problem of losses. In this respect, manufacturers either have limited

information, or at best, they rate their capacitors for special tasks, which do not necessarily coincide with the contemplated MPD applications.

For these reasons, we proceeded with our own laboratory tests of many individual capacitors, representative of all three types considered above. These tests and the corresponding results are discussed below.

B. CAPACITOR LOSSES

This topic is quite important in the evaluation of capacitors for two reasons. First, a lossy capacitor becomes an inefficient storage unit, lowering the overall efficiency of the system, and second, the life-expectancy of such a capacitor in repetitive discharge duty is sharply reduced, if any appreciable dissipation drives the internal temperature up by 30^{o} to 40^{o} C above room temperature. This second reason is quite important.

The terminology "appreciable dissipation" requires some clarification. Thus a dissipation as low as 0.1 percent may be too high for a compact capacitor with high power density, while on the other hand, a dissipation as high as 10 percent could be tolerated in a capacitor free of size and weight limitations. Generally speaking, in capacitors, where both size and weight are important, losses of the order of 0.1 percent are considered acceptable, while losses of the order of 10 percent are considered too high.

Capacitor losses have two origins: dielectric and purely ohmic. The dielectric losses are adequately described by the so called loss angle, δ . In essence, for a capacitor with instantaneous voltage and current given by V and i , the instantaneous dielectric loss is given by:

$$\text{(Diel. Loss)} = i.V.\sin\delta \simeq i.V.\delta \qquad \text{(A-1)}$$

The ohmic losses in a capacitor may be represented by an ohmic resistance R*, such that the instantaneous ohmic dissipation is given by:

$$\text{(Ohmic Loss)} = i^2R^* \qquad \text{(A-2)}$$

The total instantaneous loss is simply the sum of Eq. (A-2) and Eq. (A-3), namely:

$$\text{(Total Loss)} = i.V.\delta + i^2R^* \qquad \text{(A-3)}$$

Thus, to determine properly the energy lost per capacitor discharge (or charge), Eq. (A-3) must be integrated in time between two relevant limits. In this integration, the detailed waveforms for i and V must be taken into account. Furthermore, strictly speaking, the loss angle is not a constant but a function of frequency and thus of time.

In several cases, the dependence of the loss angle on frequency is not very strong and we may treat it as a constant. Moreover, the current through the capacitor is fairly well approximated by: $i = -C(dV/dt)$, except when the losses are very large. Under such conditions, the dielectric loss given by Eq. (A-1), or alternatively the first term in Eq. (A-3) may be integrated for any arbitrary waveform of charge or discharge. The result for discharging from a voltage V_o to zero is: $\delta\,(\frac{1}{2}CV_o^2)$. Thus the relative dielectric loss per discharge is seen to

be equal to δ , since $(\frac{1}{2}CV_o^2)$ is recognized as the stored energy. A similar argument holds for charging the capacitor from zero to V_o. Accordingly, we may consider 2δ as an approximate figure of the relative dielectric loss per charge-discharge cycle.

Regarding now the ohmic loss, the integral of i^2R^*dt over a discharge cycle may not be evaluated unless the waveform of i is known. However, for a single capacitor discharging into an ohmic load R, the energy delivered to the load is the integral of $i^2R\,dt$, over the discharge. This clearly indicates the relative loss during the discharge is $R^*/(R^*+R)$. This relative loss becomes more meaningful if we multiply both numerator and denominator by the capacitance C. Thus, the relative ohmic loss becomes $R^*C/(R^*C+RC)$. Now, we remark that R^*C is a quantity representative of any given capacitor construction. This quantity remains constant whenever several capacitors of a given construction are combined in parallel (R^* decreases while C increases proportionately). A series combination also leaves R^*C unchanged. Accordingly, we treat R^*C as a fundamental time constant associated with a given type of capacitor construction.

Furthermore, for all practical purposes, RC represents the discharge duration for all cases, except the cases of serious underdamping, which are of no interest here. Thus, the relative ohmic loss for a single capacitor may be written, in more universal terms, as $R^*C/(R^*C+t')$, where t' is the discharge time. A similar term may be written for the

charging case, but this is negligible, since charging times are much longer than t' in the cases of our interest.

To summarize then, the total relative loss of a single capacitor in a charge-discharge cycle is given by:

$$(\text{Loss})_{\text{single}} = 2\delta + [R^*C/(R^*C + t')] \qquad \text{(A-4)}$$

where the factor of 2 accounts for the dielectric loss in both the charge and discharge phases. As mentioned, t' is the discharge time.

When a capacitor or a combination of capacitors form a section of a PFN similar procedures may be followed, but the more complicated and individual waveforms must be taken into account. A practical and informative approximation is to replace the discharge time, t', of the single capacitor case with (t'/n), where now t' is the pulse duration and n is the number of sections for the complete PFN. This approximation is acceptable, given that in a PFN the load current is not provided simultaneously by all sections, but rather one section at a time provides the largest fraction of the load current. Thus in the case of a PFN, we may write:

$$(\text{Loss})_{\text{PFN}} = 2\delta + [nR^*C/(nR^*C+t')] \qquad \text{(A-5)}$$

where R^*C is a constant of the capacitance per section.

C. EVALUATION OF CAPACITOR LOSSES

With either approximation Eq. (A-4) or Eq. (A-5), whichever is more relevant, we may proceed and evaluate the losses associated with any given capacitor for a given application. The application is naturally specified by the discharge duration, or pulse duration, t' , and by the number, n , of sections we desire in a PFN. Moreover, any given capacitor (as well as a paraller and/or series combination of given capacitors) is characterized by the two coefficients δ and R*C. The first is naturally the loss angle of the dielectric, while the constant R*C (which has the dimensions of time) is characteristic of the capacitor construction, thickness of the electrode foil, etc.

Before we proceed further, we would like to relate our description of capacitor losses with the concept of the so called equivalent series resistance (ESR), which is used mostly in connection with sinusoidal waveforms. By definition,

$$D = \omega C R_s \qquad \text{(A-6)}$$

where D is the power loss factor for the capacitor. Relation (A-6) expresses simply the fact that the power loss factor in a capacitor is the ratio of the equivalent series resistance, R_s , to the capacitor reactance. In our own description we split the power loss factor, D. For a capacitor subject to sinusoidal waveforms, the power loss factor, D , has two components. One is the dielectric loss angle, δ , and the second arises from the ohmic resistance R* of the conducting parts of the capacitor.

For sinusoidal waveforms, the purely ohmic loss is given by $R^*/(1/\omega C)$ which is the ratio of the purely ohmic resistance to the reactance of the capacitor. Thus:

$$D = \delta + \omega C R^* \tag{A-7}$$

After combining Eqs. (A-6) and (A-7), we obtain:

$$R_s = (\delta/\omega C) + R^* \tag{A-8}$$

Accordingly, we see that the equivalent series resistance is not, strictly speaking, the ohmic resistance of a capacitor. Moreover, it is frequency dependent and has a well defined meaning but only for sinusoidal waveforms.

Regarding capacitor losses, manufacturers specify at most the equivalent series resistance at 60 or 120 Hz. This at best, through Eq. (A-6), gives a measure of the capacitor losses, only when the capacitor is used with sinusoidal waveforms at the specified frequency. However, the determination of the capacitor losses in applications of our interest should be carried out according to either Eq. (A-4) or Eq. (A-5), and this requires a knowledge of the constants δ and R^*C.

Thus, we proceed to evaluate these constants. A first idea may be obtained from information supplied by the manufacturer. Most manufacturers specify the dielectric used in their capacitors and the corresponding dielectric loss angle, at a given frequency, usually 60 Hz. Additional information may be obtained from handbooks on dielectrics. Furthermore, manufacturers may supply information regarding the geometry

of their capacitors, the electrode foil and the electrode connections. From this information, a very rough idea of R^* may be obtained.

In our laboratory, we have derived more reliable information on both dielectric and ohmic losses using the following methods.

1. Calorimetric Method

This method is in essence a full-dress rehearsal. The capacitor under test is cycled (charge-discharge) repetitively with known voltage and current waveforms at known rep rates. The capacitor is contained within a calibrated airstream calorimeter, appropriately insulated. In the steady state, the power dissipated in the capacitor is eventually carried away by the airstream and measured. The measured average power loss, divided by the known rep rate, determines the energy, E, dissipated in the capacitor in a complete charge-discharge period. This then may be related to the capacitor loss constants, δ and R^*, as follows.

Consider Eq. (A-3), which gives the total instantaneous power loss in the capacitor. After integration over a complete period, we may obtain:

$$E_1 = \left[\int iV\,dt\right]_1 \cdot \delta + \left[\int i^2\,dt\right]_1 \cdot R^* \qquad \text{(A-9)}$$

Here, the subscript 1 designates any set of charge-discharge waveforms of our choice, and hence the integrals are known. If, in

addition to Eq. (A-9), another set, say No. 2 of a known waveform is used and the corresponding energy loss per period is measured, then:

$$E_2 = \left[\int iV dt\right]_2 \cdot \delta + \left[\int i^2 dt\right]_2 \cdot R^* \qquad \text{(A-10)}$$

where again the known waveforms are integrated over a complete charge-discharge period.

Equations (A-9) and (A-10) may be solved simultaneously to yield the desirable loss coefficients δ and R^* for any capacitor of our interest. In practice, more than two sets of waveforms may be used and the additional equations may provide more accuracy if desired. In our experimental procedures, we used mostly two sets of waveforms. One set was the ordinarily available 60 Hz, sinusoidal, at various voltages up to 1000 volts. The second set was a slow charge, fast discharge routine (discharge times of the order of 100 microseconds) at any desirable rep rate up to 60 pps. The various capacitors under test handled powers ranging from a few hundred watts to 10 kilowatts and the measured power losses ranged between a few parts per ten thousand to a few percent. Representative results will be presented shortly in tables.

The calorimetric method under consideration here is very desirable, since it is as close to actual conditions as is possible in a laboratory. However, the method has its limitations, especially

in the evaluation of capacitors with relatively small losses. In such cases, the time required for steady state is impractically long (e.g., one or a few days) and hour-to-hour or day-to-day temperature drifts may interfere. Moreover, calorimeters of this type are not very reliable when power losses lower than one or a few watts are considered.

2. Signal Method

This method is distinguished from the calorimetric method by the fact that the waveforms used in the capacitor contain powers which are orders of magnitude lower. Here, in essence, the capacitor under test becomes one of the arms of a sensitive bridge which, when driven by a sinusoidal signal, measures the appropriate phase difference between current and voltage. This, in turn, is directly identified with the power loss factor, D, occurring in either Eq. (A-6) or Eq. (A-7).

Of particular interest here is Eq. (A-7), which represents a straight line if the measured values of D are plotted as a function of frequency. Clearly, the intercept of this straight line is a measure of the dielectric loss angle, while from the slope we may determine the resistance, R^*, of any known capacitor, C.

In our laboratory practice, we employ an accurate bridge (General Radio Impedance Bridge, type 1608-A) with the appropriate modification for external drive by a stable oscillator, at any

desirable frequency. Usually the frequencies between 10 and 10^4 Hz are the most useful. Further provisions are made for dc-biasing of capacitors up to 500 volts. This is necessary for the evaluation of electrolytic capacitors by the signal method.

Examples of capacitor evaluation by the signal method are illustrated in figs. A-1, A-2 and A-3, respectively for a very good, an acceptable and a very lossy capacitor. Alternatively, these capacitors are generally characterized as Type (a), (b) and (c), as discussed earlier. In the tests of the electrolytic capacitors, see fig. A-3, a dc bias was used, both at 6 and at 300 volts, without noticeable differences.

The great attraction of the signal method is that the loss coefficients of a capacitor (both dielectric and ohmic) may be determined with adequate reliability in a matter of a few minutes. Naturally, a sufficiently sensitive and accurate bridge must be available and a few modifications are necessary for external frequency drive and for dc bias. Moreover, the dependence of the dielectric loss on frequency is easily detected by serious deviations of the measured power loss factor from the straight line behavior described by Eq. (A-7) and illustrated in figs. A-1, A-2, and A-3.

The limitations of the signal method are felt, as expected, with the very good capacitors which have very small dielectric and ohmic losses. In this sense the capacitor under evaluation is, so

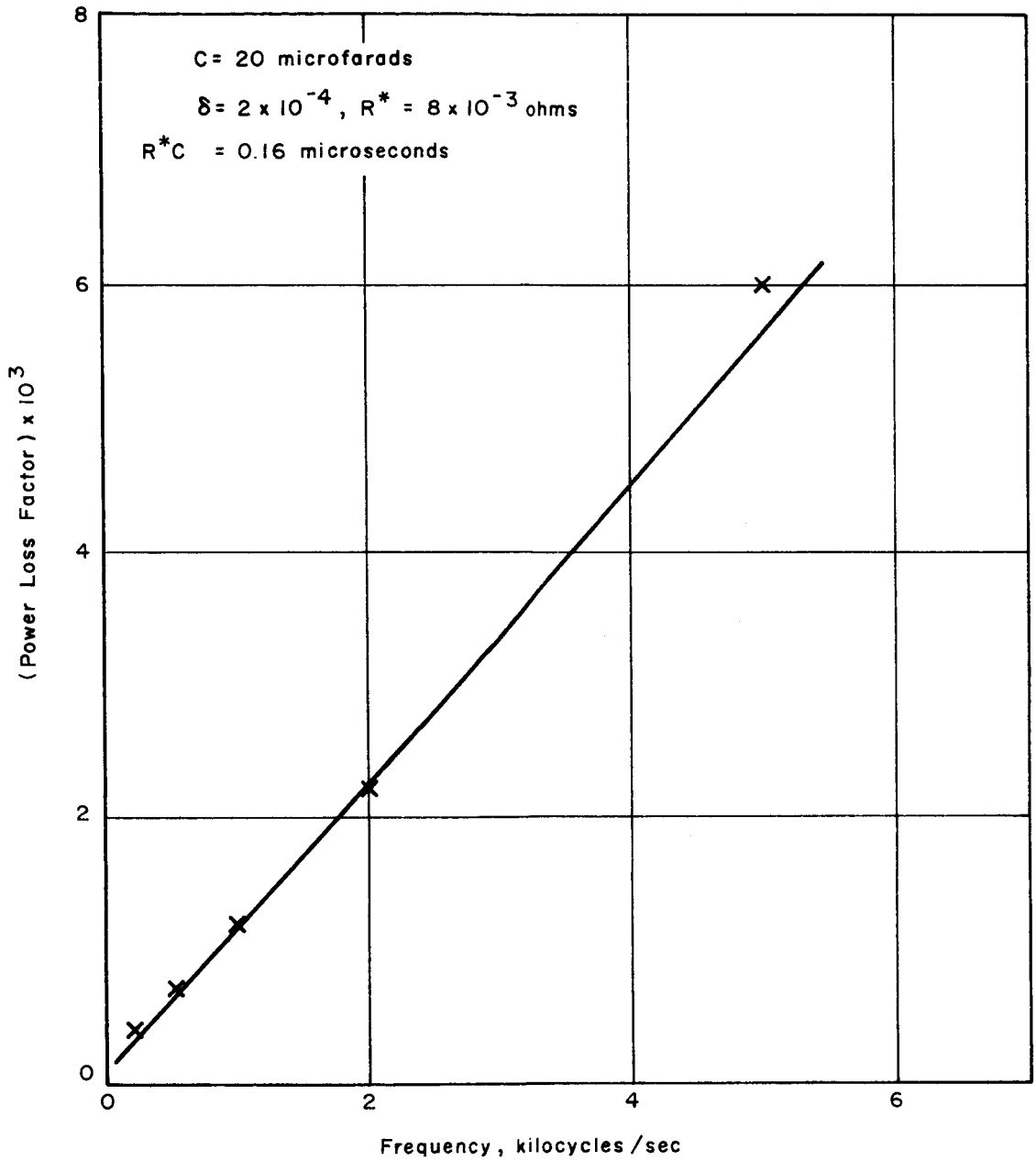

Figure A-1 POWER LOSS FACTOR VERSUS FREQUENCY
G.E. Capacitor, (Polycarbonate
Film, Extended Foil).

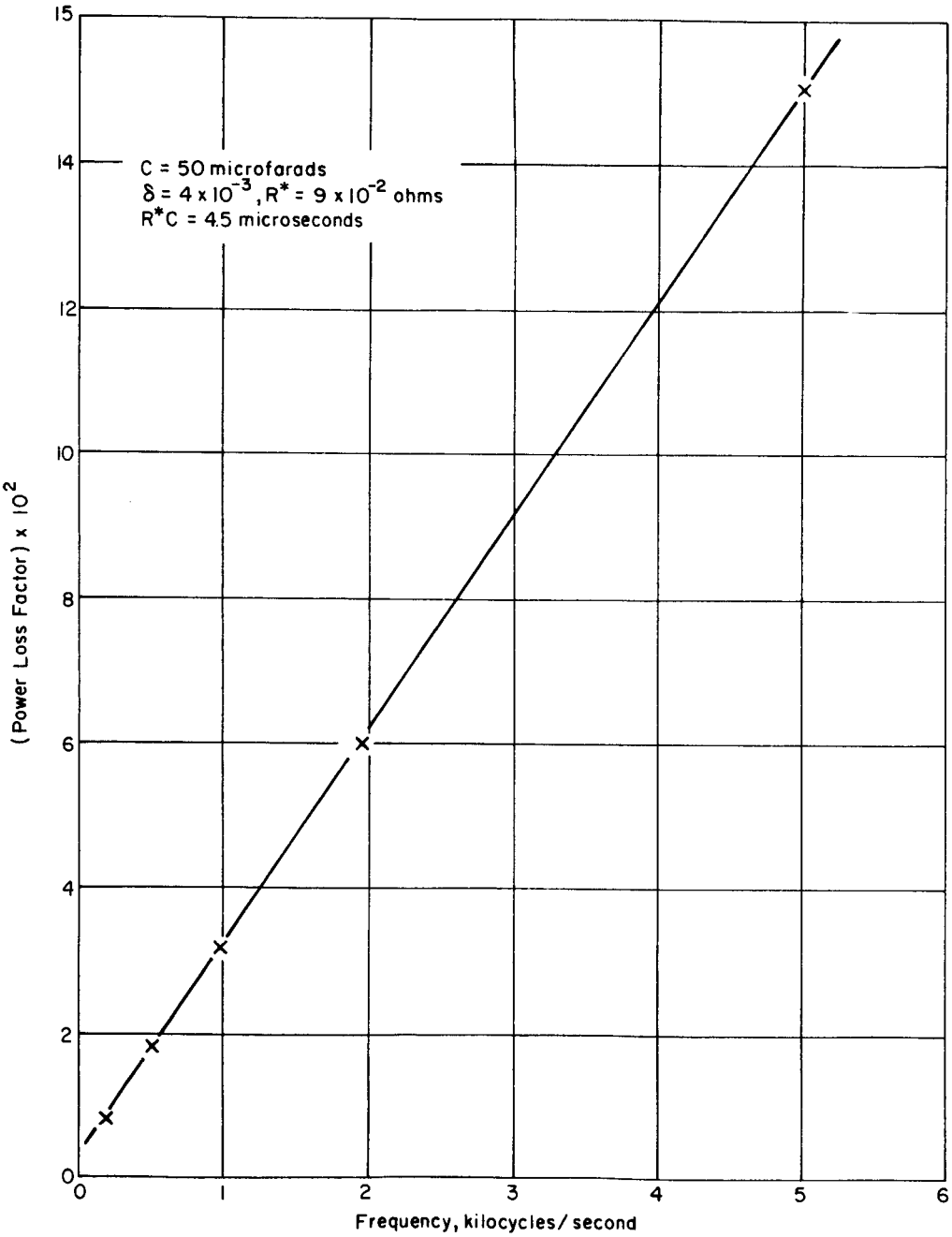

Figure A–2 POWER LOSS FACTOR VERSUS FREQUENCY
G.E. Capacitor, (Paper Dielectric, No Extended Foil)

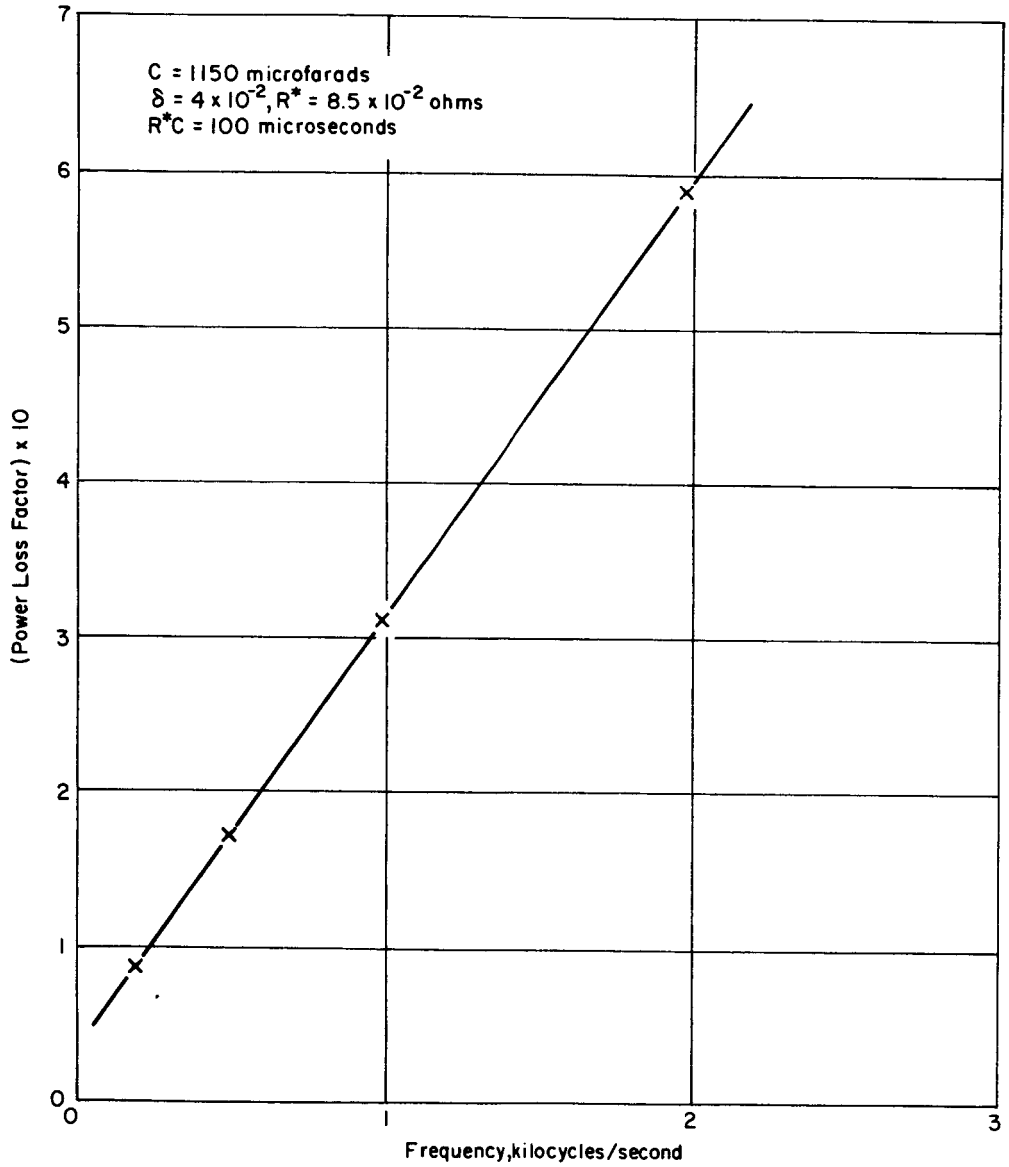

Figure A–3 POWER LOSS FACTOR VERSUS FREQUENCY
Sprague, Electrolytic Capacitor

to speak, at least as good as the special components used in an accurate, sensitive and very sophisticated bridge.

D. SUMMARY OF RESULTS

First, we wish to compare results obtained by the calorimetric method with the corresponding results obtained by the signal method. This comparison is made in table A-I, where the entries are labeled Type (a) or (b) according to our general classification, discussed earlier. For each entry, also, we specify the manufacturer and the value of the capacitance. Then the dielectric loss angles and the ohmic resistances are compared and, finally, average values are obtained for both the dielectric loss and for the time constant, characteristic of the ohmic losses.

For the first two entries, no calorimetric data could be obtained because of too small losses. The agreement between the two methods is not excellent, but should be considered satisfactory since most of the capacitors under comparison have rather small losses which may not be determined with high accuracy. (The agreement regarding the ohmic losses is much better than for the dielectric losses.)

The substantial differences appearing in the dielectric losses are not totally unexpected. In our evaluation, we treat the dielectric loss angle as independent of frequency and temperature. In reality this is not true, and in our tests, a temperature dependence may very well enter

TABLE A–I

COMPARISON OF RESULTS FROM THE EVALUATION OF CAPACITOR LOSSES BY TWO DIFFERENT METHODS

Classification	Manufacturer	C, μfd.	Calorimeter Method		Signal Method		Averages	
			δ, 10^{-4}	R* milliohms	δ, 10^{-4}	R*, milliohms	δ, 10^{-4}	R*C, μsec
Type (a)	G.E.	20	--	--	2	8	2	0.16
Type (a)	Maxwell	35	--	--	10	9	10	0.32
Type (a)	Maxwell	105	9	3.5	13	5	11	0.44
Type (a)	G.E.	21	9	13	22	11	15	0.25
Type (b)	G.E.	51	34	50	30	52	32	2.60
Type (b)	G.E.	50	42	94	35	90	39	4.70
Type (b)	Sprague	95	110	18	50	23	80	2.00

in the calorimetric method, while frequency dependence is obviously relevant in both methods.

With the mentioned uncertainties in mind, we proceeded to evaluate a large number of various capacitors of all three types: (a), (b) and (c). We applied mostly the signal method and used the calorimetric method for occasional checks. Our results may be generalized by the parameters tabulated in table A-II below:

TABLE A-II

RELATIVE DIELECTRIC AND OHMIC LOSSES FOR THREE GENERALIZED TYPES OF CAPACITORS

Capacitor	δ, percent	R*C μsec
Type (a)	0.02 to 0.2	0.2 to 0.5
Type (b)	0.4 to 0.8	2.0 to 5.0
Type (c)	4.0 to 6.0	100

These results are valid for frequencies from 10 to 10^4 Hz and temperatures in the vicinity of room temperature. At higher temperatures the ohmic losses do not change appreciably. The same is true for lower temperatures, except for the losses of electrolytic capacitors, which increase sharply.

Consider now the application of the capacitors in question in the case of a pulse forming network with, say, n = 5 sections, and with a pulse duration of the order of a millisecond. From Eq. (A-5) and the

results of table A-II, we see that the relative losses of Type (a), (b) and (c) capacitors are respectively less than 1 percent, about 1 percent and well above 10 percent. Thus, for applications of our interest and from the viewpoint of losses, the capacitor types under consideration may be classified as very good, acceptable and very lossy.

It must be noted here that a capacitor with low losses does not necessarily have a low energy density. It is true that the G.E. capacitors, in the first and fourth entry of table A-I, are heavy, but these capacitors have been designed for fast SCR commutation duty and not, strictly speaking, for energy storage. However, note that the Maxwell capacitors, in the second and third entries of table A-I, have low losses and at the same time their corresponding energy densities are 125 and 64 joule/lb.

In conclusion, the losses of a capacitor are determined primarily by the materials and construction detail and secondarily by the contemplated application. This problem is in principle uncoupled and, to a good extent, may be treated separately from the problem of energy density.

E. SPECIFIC WEIGHT AND LIFE-EXPECTANCY CONSIDERATIONS

The question of specific weight, or energy density, of commercially available capacitors is now considered. We have found this problem to be much less analytically tractable and more inadequately documented than the problem of losses. Empirical documentation is especially poor,

when the specific weight problem is coupled to the question of life expectancy, in terms of total number of pulse discharges. Here, data on life expectancy, up to 10^3 to 10^4 pulses, appear to be fairly well documented and are relatively easy to check. However, no real test data appear to be available, regarding the life-expectancy versus voltage-derating relation, for life expectancies up to or beyond 10^7 pulses.

Most manufacturers have limited test data, mostly at much lower life expectancies. They appear to extrapolate to higher numbers of pulses, mainly on the basis of better known relations, regarding dc life expectancies. The validity of this extrapolation, for the case of pulse-discharge duty, is very much in doubt, with the uncertainties becoming increasingly larger as the total number of pulses increases.

It is also true that the life expectancy for pulse-discharge duty is a poorly known function of several additional constraints, such as voltage reversal per discharge, pulse duration, rep rate, ambient temperature, etc. Accordingly, generalizations are not available and may not be easily established without a rather extensive and expensive test effort.

Generally speaking, specific weights as small as 0.01 to 0.02 lb/joule (or 50 to 100 joule/lb) appear feasible according to claims of reputable manufacturers. Examples are the capacitors in the second and third entry of table A-I. The conditions attached to the mentioned specific weights are storage at a few kilovolts and operation with less

than 20 percent voltage reversal at room temperatures. Under such conditions, a life expectancy in the range 5×10^3 to 10^4 pulses is considered possible, with a reliability figure of about 90 percent.

Any deviation from the aforementioned conditions tends to reduce the life expectancy, or alternatively, to increase the specific weight. The temperature dependence is particularly sensitive, and the life expectancy is sharply reduced, as the temperature increases even by few tens of degrees centigrade.

As mentioned, life expectancy may be increased, virtually indefinitely, provided that the capacitor is derated in charging voltage. Most reputable manufacturers suggest that an extension of life expectancy by two orders of magnitude may be accomplished when the charging voltage is lowered by a factor of 2. Alternatively, this means a derating of the specific weight by a factor of 4. However, refer to the remarks made earlier in this section, regarding the credibility and the difficulties of establishing the relationship between life expectancy and specific weight.

In conclusion then, according to the present state of the art for commercially available capacitors, an extension of the pulse life expectancy from the $10^3 - 10^4$ range to the $10^7 - 10^8$ range will require a voltage derating by a factor of 4, or alternatively, an energy density reduction by a factor of 16. In other words, numbers such as 3 to 6 joule/lb would be relevant.

So far, our remarks about specific weight refer to the less lossy types of capacitors, in table A-II, especially to Type (a), which are also compatible with high rep rates and higher power densities. For electrolytic capacitors, specific weights as low as 0.01 lb/joule are acceptable for dc duty, in power-supply filter applications. However, specific weight ratings and life-expectancy data are generally not available for electrolytic capacitors in pulse discharge duty. These capacitors are too lossy for such duty, unless they are discharged in times much longer than a millisecond. (See Eq. (A-5) and table (A-II.)

DISTRIBUTION LIST

Addressee	No. Copies
NASA Langley Research Center Hampton, Virginia 23365	
Attn: Program Reports & Analysis Unit, Mail Stop 122	4
Raymond L. Zavasky, Mail Stop 110	1
Joseph Burlock, Mail Stop 160	25
Robert V. Hess, Mail Stop 160	1
Macon C. Ellis, Jr., Mail Stop 186	1
NASA Ames Research Center Moffett Field, California 94035	
Attn: Library, Mail Stop 202-3	1
Howard A. Stine, Mail Stop 229-2	1
Dr. Frederico G. Casal, Mail Stop 202-8	1
NASA Flight Research Center P. O. Box 273 Edwards, California 93523	
Attn: Library	1
Jet Propulsion Laboratory 4800 Oak Grove Drive Pasadena, California 91103	
Attn: Library, Mail 111-113	1
Dr. Noble M. Nerheim, Mail 122-123	1
Daniel J. Kerrisk, Mail 122-123	1
NASA Manned Spacecraft Center 2101 Webster Seabrook Road Houston, Texas 77058	
Attn: Library, Code BM6	1
NASA Marshall Space Flight Center Huntsville, Alabama 35812	
Attn: Library	1
Ernst Stuhlinger, AD-S	1
Gerhard B. Heller, S&E-SSL-DIR	1
Wallops Station Wallops Island, Virginia 23337	
Attn: Library	1

DISTRIBUTION LIST (cont)

Addressee	No. Copies
NASA Lewis Research Center 21000 Brookpark Road Cleveland, Ohio 44135	
Attention: Library, Mail Stop 60-3	1
Research Support Procurement Section, Mail Stop 500-312	1
Technology Utilization Office, Mail Stop 3-19	1
Management Services Division, Mail Stop 5-5	1
Report Control Office, Mail Stop 5-5	1
Channing C. Conger, Mail Stop 54-1	1
Henry R. Hunczak, Mail Stop 54-51	
Stanley Domitz, Mail Stop 54-5	1
Edward W. Otto, Mail Stop 54-1	1
Wolfgang E. Moeckel, Mail Stop 301-1	1
George R. Seikel, Mail Stop 301-1	1
Dennis J. Connolly, Mail Stop 301-1	1
NASA Goddard Space Flight Center Greenbelt, MD. 20771	
Attention: Library	1
William C. Isley, Code 734	1
John F. Kennedy Space Center Kennedy Space Center, FL 32899	
Attention: Library, Code IS-CAS-42B	1
National Aeronautics and Space Administration Washington, DC 20546	
Attention: Library, Code KSS-10	1
NASA Code RP	1
James Lazar, Code KSS-10	1
Dr. Karlheinz Thom, Code RRE	1
Jerome P. Mullin, Code RNT	1
Plasma Physics Engineering Laboratory State University of New York at Buffalo Buffalo, NY 14214	
Attention: Dr. D. M. Benenson	1

DISTRIBUTION LIST (cont)

Addressee	No. Copies
Hughes Research Laboratories Ion Physics Department 301 Malibu Canyon Road Mailibu, CA 90265 Attention: Jerome H. Molitar	1
North Carolina State University Raleigh, NC 27607 Attention: Professor H. A. Hassan	1
Comsat Laboratories Positioning and Orientation Branch Washington, DC 20013 Attention: Bernard Free	1
Princeton University Guggenheim Laboratories James Forrestal Campus Princeton, NJ 08540 Attention: Woldemar F. von Jaskowsky	1
TRW Systems Inc. One Space Park Redondo Beach, CA 90278 Attention: Dr. C. L. Dailey Dr. J. M. Sellen	1 1
Electro-Optical Systems Inc. Electric Propulsion Applications Office 306 North Halsted Street Pasadena, CA 91109 Attention: Ronald S. H. Toms G. L. Cann	1 1
Republic Aviation Farmingdale, Long Island, NY 11735 Attention: William J. Guman, Head, Electric Propulsion Power Conversion Division	1
Air Force Weapons Laboratory Kirtland Air Force Base, NM 87417 Attention: WLPC/Capt. C. F. Ellis	1

DISTRIBUTION LIST (cont)

Addressee	No. Copies
Thermal Mechanical Research Laboratory OAR USAF Wright-Patterson Air Force Base, OH 45433 Attention: Eric Soehngen	1
Case Institute of Technology 10900 Euclid Avenue Cleveland, OH 44106 Attention: Professor O. K. Mawardi Dr. Eli Reshotko	1 1
Catholic University of America Department of Space Sciences and Applied Physics Washington, DC 20017 Attention: Professor C. C. Chang	1
University of Minnesota Department of Mechanical Engineering Heat Transfer Laboratory Minneapolis, MN 55435 Attention: Dr. E. Pfender	
Avco Corporation Avco Everett Research Laboratory 2385 Revere Beach Parkway Everett, MA 02149 Attention: Dr. R. M. Patrick	1
General Electric Company Missile and Space Division Space Sciences Laboratory P. O. Box 8555 Philadelphia, PA 19101 Attention: T. Karns	1
Los Alamos Scientific Laboratories P. O. Box 1663 Los Alamos, NM 87544 Attention: Dr. Stratton	1
Westinghouse Astronuclear Laboratories Electric Propulsion Laboratories Pittsburgh, PA 15234	1

DISTRIBUTION LIST (cont)

Addressee	No. Copies
Avco Corporation Research & Advanced Development Division 201 Lowell Street Wilmington, MA 01887	
Attention: R. R. John	1
S. Bennett	1
A. C. Malliaris	1
University of California, San Diego LaJolla, CA 92037	
Attention: Professor R. Lovberg	1
Colorado State University Fort Collins, CO 80521	
Attention: Professor W. Mickelsen	1
Research and Technology Division Wright-Patterson Air Force Base, OH 45433	
Attention: David Fritts, AFAPL (APIE-1)	1
United States Air Force Office of Scientific Research Washington, DC 20025	
Attention: M. Slawsky	1
Princeton University Forrestal Research Center Princeton, NJ 08540	
Attention: Dr. R. G. Jahn	1
Aerospace Corporation P. O. Box 95085 Los Angeles, CA 90045	
Attention: Library/Technical Documents Group	1
General Dynamics Convair Division San Diego, CA 92112	
Attention: Dr. A. V. Larson	1

DISTRIBUTION LIST (Concl'd)

Addressee	No. Copies
Giannini Scientific Corporation 3839 South Main Street Santa Ana, CA 92702 Attention: Adriano Ducati	1
NASA Scientific and Technical Information Facility P. O. Box 33 College Park, MD 20740	(+1 vellum) 5